# Compartment-specific plasticity in the lateral amygdala during fear learning

***Inauguraldissertation***

*Zur*

*Erlangung der Würde eines Doktors der Philosophie*

*vorgelegt der*

*Philosophisch-Naturwissenschaftlichen Fakultät*

*der Universität Basel*

*von*

Simon d'Aquin

aus Frankreich

*Basel, 2021*

*Genehmigt von der Philosophisch-Naturwissenschaftlichen Fakultät*

*auf Antrag von*

**Prof. Dr. Andreas Lüthi**

(Fakultätsverantwortlicher und Dissertationsleiter)

**Prof. Dr. Tiago Branco**

(Korreferent)

Basel, 15th December 2020

**Prof. Dr. Martin Spiess**

(Dekan)

# Table of Contents

# Abstract

Local dendritic integration of synaptic inputs crucially shapes somatic output. While work *in vitro* has provided valuable insights into the mechanisms underlying dendritic integration, how experience affects the relationship between behaviorally relevant somatic and dendritic activity in single neurons remains largely unknown. Using deep brain two-photon $Ca^{2+}$ imaging, we investigate how sensory stimuli are represented in somata and dendrites of Lateral Amygdala principal neurons and how these representations develop over the course of auditory fear learning. We observe a higher rate of dendrite-specific activity during tone presentations in naïve animals, which was abolished by chemogenetic inhibition of somatostatin-expressing interneurons, suggesting that these neurons gate dendritic integration of tone inputs. We also find that fear learning induces tone response plasticity that is bidirectional in somata but largely unidirectional in dendrites and identified a neuronal population with uncoupled somatic and dendritic plasticity of tone response. Overall, our results indicate that fear learning induces compartment-specific plasticity and suggests that inputs conveying tone information are processed locally in the amygdala during auditory fear learning.

# Abbreviations

| | |
|---|---|
| AAV | Adeno-associated virus |
| AMPAR | α-amino-3-hydroxy-5-methyl-4-isoxazolepropionic acid receptor |
| AP | Antero-posterior axis |
| BA | Basal amygdala |
| bAP | back-propagating action potential |
| BLA | Basolateral amygdala |
| BM | Basomedial amygdala |
| BNST | Bed nucleus of the stria terminalis |
| CaMKII | Calmodulin-dependent protein kinase II |
| CCK | Cholecystokinin |
| CeA | Central amygdala |
| CNO | Clozapine N-oxide |
| Cre | Cre recombinase |
| CS | Conditioned stimulus |
| CSdown | Downregulated by CS |
| CSup | Upregulated by CS |
| DREADD | Designer receptor exclusively activated by designer drugs |
| DV | Dorso-ventral axis |
| Flp | Flippase (recombinase) |
| fMRI | Functional magnetic resonance imaging |
| GABA | γ-aminobutyric acid |
| GRIN | Grinded index (lens) |
| IP | Intraperitoneal |
| ITI | Inter trial interval |
| L5 | Cortical neuronal layer 5 |
| LA | Lateral amygdala |
| LTD | Long-term depression |
| LTP | Long-term potentiation |
| ML | Medio-lateral axis |
| NA | Numerical aperture |
| NAc | Nucleus accumbens |
| NMRAR | N-methyl-D-aspartate receptor |
| PAG | Periaqueductal gray |
| PFC | Prefrontal cortex |
| PKCd | Protein kinase C delta |
| PN | Principal neuron |
| PV | Parvalbumin |
| SD | Standard deviation |
| SN | Substantia nigra |
| SST | Somatostatin |
| STDP | Spike-timing-dependent plasticity |
| US | Unconditioned stimulus |
| VIP | Vasoactive intestinal peptide |

# Introduction

## Understanding learning

For animals and humans, learning can be defined as the process of acquiring new behaviors, skills or knowledge and understanding through experience and interaction with the environment. The ability to learn is a defining feature of nervous systems, with simple organisms displaying some forms of learning (Fig. 1). Simple associations such as the smell of a food source and its availability, remembering the location of a nest or learning new motor skills all involve the formation, storage and retrieval of a memory, be it conscious or unconscious. Different types of learning provide organisms with the ability to adapt and interact with their environment in ways that are beneficial to their survival. During associative learning, an organism learns the causal relationship between two events or stimuli, such as how the color of an edible fruit relates to its taste (*1*).

Furthermore, learning can also be non-associative, resulting from habituation or sensitization to a repeated stimulus. A role for habituation can be to disregard stimuli that occur frequently in the environment but that do not carry any consequences for the animal to attend to, such as the sound of the wind in the trees (*2*). More generally, in order for learning to occur, new memories must be formed and stored in the nervous system and eventually expressed through behavior.

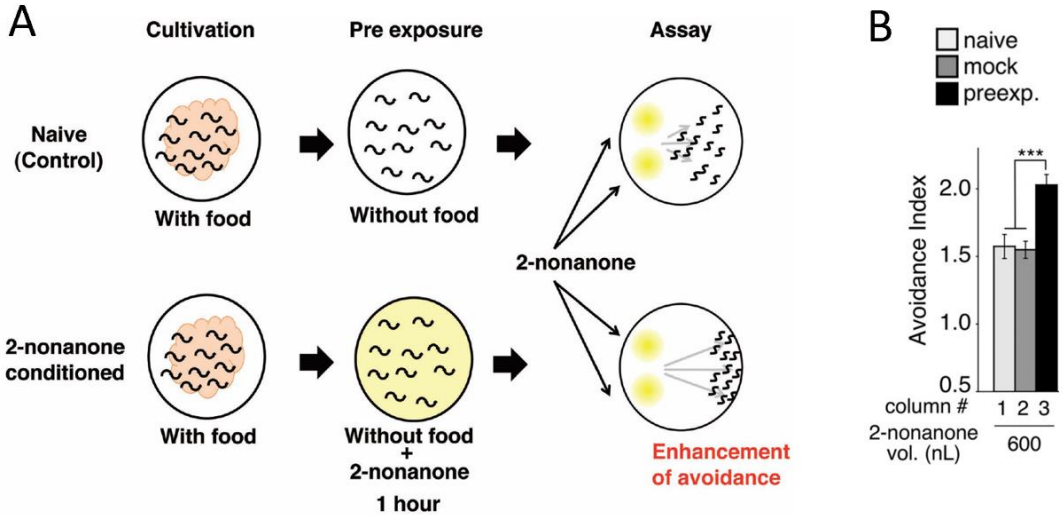

**Fig. 1. The worm C. elegans is capable of associative learning.**

**(A)** top, food-deprived worms avoid the new chemical 2-nonanone. Bottom, food-deprived worms in the presence of 2-nonanone show enhanced avoidance of the chemical later on, during the assay. **(B)** higher avoidance in worms pre-exposed to 2-nonanone than in naïve worms, indicating that worms associated this chemical with the absence of food (*3*).

Learning results from physical changes in the nervous system that ultimately lead to a given sensory stimulus resulting in different behaviors. In other words, learning is implemented through persistent modifications of the input-output relationship of the nervous system. Neuroscience as a field aims to understand the biological processes that underlie learning from a mechanistic perspective.

In 1982, David Marr stated three levels at which an information-processing task must be understood: (a) at a computational level - understanding formally what problems the system is trying to solve; (b) at an algorithmic level – the mathematical/computational solutions adopted by the system; and (c) at an implementational level - how these mathematical operations are achieved by biological and neuronal "hardware" (*4*).

According to Marr, a true understanding of how brains learn can only be achieved if a theory can be formulated that spans all three levels and give rise to predictions that can be verified experimentally.

## Learning frameworks

Many models have been developed that aim at describing how the brain carries out learning. The models introduced below are not necessarily mutually exclusive, as different brain areas, neuronal microcircuits or cell types might implement diverse combinations of them. As a result, identifying the principles of information processing in the brain has remained a challenging task. With recent advances in the emerging fields of artificial neuronal network and machine learning, a flurry of new models have arisen with putative biological relevance, although their level of abstraction often renders biological experimentation difficult (*5*).

Hebbian learning

In 1949, Donald Hebb proposed a learning theory since then referred to as "Hebb's rule":

*"Let us assume that the persistence or repetition of a reverberatory activity (or "trace") tends to induce lasting cellular changes that add to its stability. ... When an axon of cell A is near enough to excite a cell B and repeatedly or persistently takes part in firing it, some growth process or metabolic change takes place in one or both cells such that A's efficiency, as one of the cells firing B, is increased."* (*6*)

This postulate, often summarized as "Neurons that fire together, wire together", has been highly influential and received much experimental support. Hebb's rule implies that cell assemblies arise from ongoing neuronal activity and can act as processing units. These ideas still hold an important place in the modern view of how the brain processes information.

The Rescorla–Wagner model

The Rescorla–Wagner model has been applied to describe the rate of learning in the context of classical conditioning, where learning is conceptualized in terms of associations between a conditioned (CS) and an unconditioned (US) stimulus (*7*). During classical conditioning, an initially neutral CS (for example, a tone) precedes an innately aversive or appetitive US (for example, a sweet fruit juice). After a few CS-US pairings, the subject learns that the CS predicts the US and develops a behavioral response to the CS alone (for example, salivating). In this model, the learning rate is updated on each CS-US paring and formalized in an equation that depends on the difference between the expected and actual US, and therefore belongs to the "prediction-error" framework category (Fig. 2A).

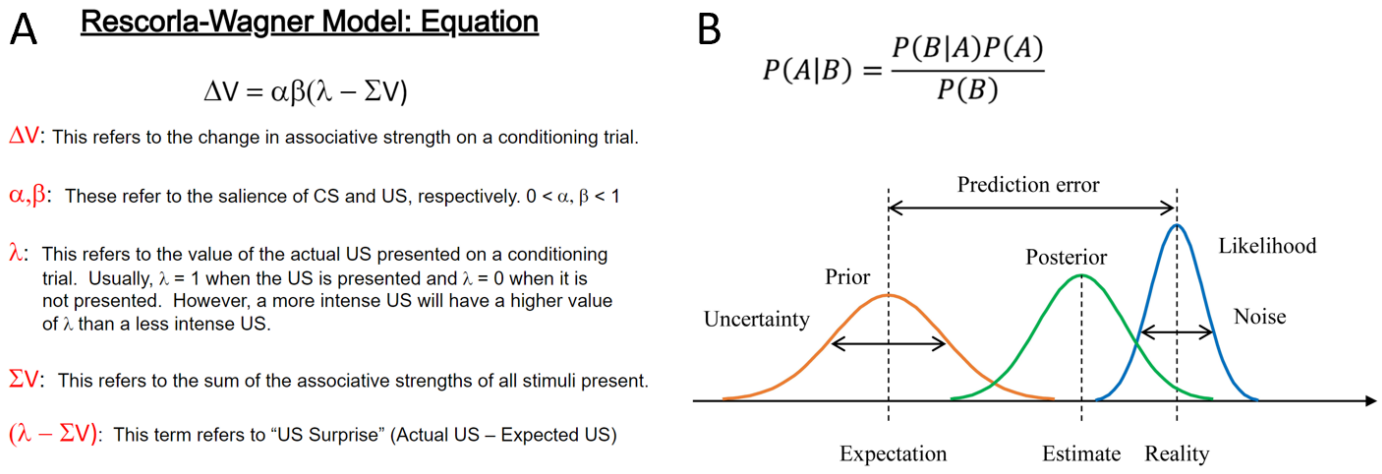


**Fig. 2. Different models can be used to describe associative learning**

**(A)** Rescorla-Wagner equation describing learning rate during conditioning.

**(B)** Bayesian inference model. Top, Bayes theorem:

- A Stands for any hypothesis whose probability may be affected by data.
- P(A), the prior probability, is the estimate of the probability of A before the data B, the current evidence, is observed.
- B is the evidence or reality and corresponds to new data that were not used in computing the prior probability.
- P(A | B), the posterior probability, is the probability of H given B, after B is observed, it is what we want to know: the probability of a hypothesis given the observed evidence.
- P(B | A) is the probability of observing B given A or likelihood.
- P(B) is sometimes termed the marginal likelihood or "model evidence". This factor does not enter into determining the relative probabilities of different hypotheses.

Bottom, schematic illustration of Bayes Theorem: prior beliefs are represented as a probability distribution. Upon new evidence (e.g. sensory input), these prior beliefs are updated into posterior beliefs (*7*).

## Reinforcement learning

Temporal difference learning involves constant ("online") updating of the prediction with new information from the environment. The firing rate of dopaminergic neurons in VTA/SN, in particular, seems to mimic the error function in the algorithm (*8*). For example, in an experiment were monkeys were trained to associate a stimulus with the reward of juice, dopamine cells initially increased firing rates when the monkey received juice, indicating a difference in expected and actual rewards. Over time this increase in firing back-propagated to the earliest reliable stimulus predictive of the reward. Once the monkey was fully trained, there was no increase in firing rate upon presentation of the predicted reward anymore. Moreover, the firing rate for the dopamine cells decreased below normal activation when the expected reward was omitted (*9*) (Fig. 3).

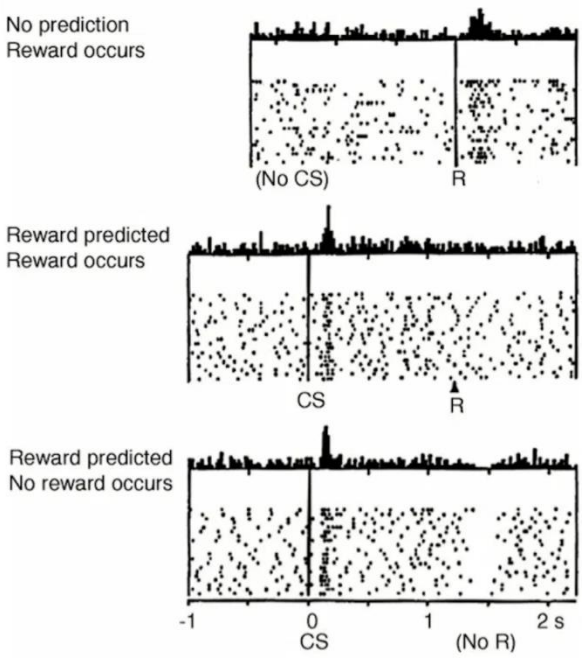


**Fig. 3. Dopaminergic neurons activity during appetitive conditioning**

The black dots represent dopaminergic neuron firing. Top, a neuron responds to unpredicted reward delivery. Middle, after conditioning, the subject learned that the CS predicts the US and the neuron fires to the CS and not anymore to the reward. Bottom, after conditioning, when the expected reward is omitted, the neuron's firing decreases below baseline (*9*).

Bayesian inference

Bayesian approaches to understand brain function formulate perception and action as inferential processes (*7*). These inferences combine "prior" beliefs with a generative (predictive) model to explain the causes of sensations and thereby offer a probabilistic approach to explain how experience can update prior beliefs (Fig. 2B).

## Fear conditioning as a model for associative learning

Fear is an emotion induced by perceived danger or threat that drives behavioral changes resulting in the active or passive avoidance of a putative source of risk. While some fears are innate (many humans are afraid of heights, darkness or animals in the absence of negative prior experience), new fears can be acquired through experience. Animals, including humans, naturally associate the context in which aversive events are experienced and reliably develop a fearful response when later exposed to a similar context. For example, after experiencing a car accident, people can develop fear to high speeds, being in a car, and even fear of cars altogether, a process termed fear generalization (*10*) .

Classical fear conditioning, a form of Pavlovian conditioning, can be performed in a laboratory setting by repeatedly pairing an initially neutral stimulus (conditioned stimulus or CS, typically a tone) with an innately aversive stimulus (unconditioned stimulus or US, typically an electrical shock). The subject gradually develops a fearful reaction to the CS as it

learns that it predicts the US (Fig. 4). Fear conditioning is a simple, reliable and tractable way to induce associative learning. It is evolutionary conserved and can be observed in worms and insects to primates, making it a highly suited paradigm to study associative learning (*3*, *11*-*13*).

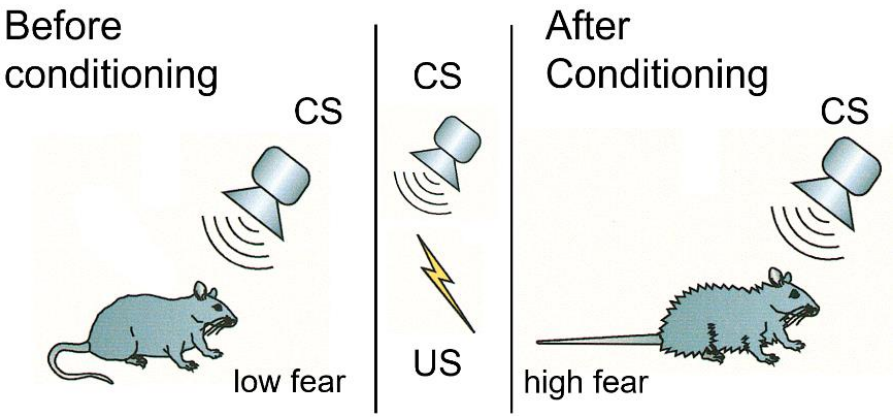


**Fig. 4. Auditory fear conditioning in rodents.**

Left, before conditioning, mice do not show physiological signs of fear to a neutral tone CS. Middle, fear conditioning consists in pairing the same CS with an aversive US, often a mild electrical foot-shock, by presenting the US right after the CS. Right, after conditioning, mice learned that the CS predicts the US ad show a freezing response to the tone (*14*).

## The Amygdala

Amygdala structure

The amygdala is located deep in the temporal lobe in humans. It is composed of a cortex-like basolateral nucleus (BLA) and a striatum-like central nucleus (CeA) (Fig. 5).

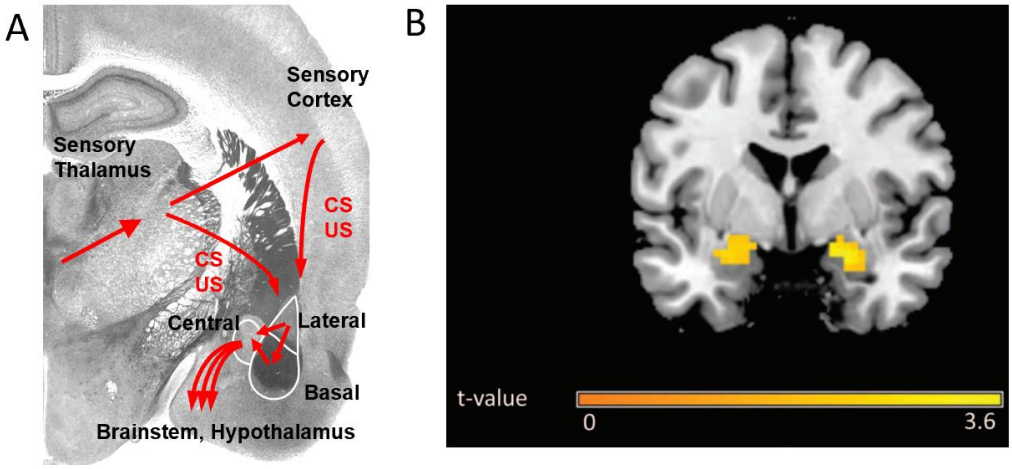


**Fig. 5. The amygdala integrates sensory inputs during fear conditioning.**

**(A)** Amygdala (simplified) circuitry. The basal and lateral amygdala receive inputs from sensory cortex and thalamus and project to the CeA. The CeA sends projects to brain areas directly involved in the control of physiological functions, including the brainstem and the hypothalamus. Arrows indicate the direction of information flow. **(B)** Bilateral amygdala activation following fear conditioning (*15*). Human patients with amygdalar lesions suffer from a range of social and emotional disorders, do not show physiological indications of conditioned fear and in extreme cases lose the ability to experience fear (*16*).

The BLA contains a majority (~80%) of glutamatergic, CaMKII-positive principal neurons (PNs) and a minority (~20%) of local GABAergic interneurons that differentially express a set of genetic markers such as parvalbumin (PV), somatostatin (SST), Vasoactive intestinal peptide (VIP) or Cholecystokinin (CCK). Interestingly, the genetic markers expressed by basolateral amygdala (BLA) neurons, the relative representations of these neurons and their connection patterns are similar to that of the neocortex but differs from it in that the BLA does is not organized by layers (Fig. 6).

The BLA can be further divided in lateral (LA), basal (BA) and basomedial (BM) nuclei. The LA is the main sensory input station of the amygdala, receiving strong projections from sensory cortices and from sensory thalamic nuclei. BA and BM are reciprocally connected with the prefrontal cortex (PFC) and the hippocampus and also project to the striatum (Nucleus accumbens (NAc), Bed nucleus of the stria terminalis (BNST)) and to the neighboring CeA. CeA principal neurons are GABAergic and differentially express the genetic markers Corticotropin-releasing factor (CRF), CCK, SST or protein kinase C $\delta$ (PKCd) (*17*).

The CeA is regarded as the main output of the amygdala and contacts brainstem nuclei, the Periaqueductal gray (PAG), the lateral hypothalamus and the BNST, all regions that can exert control over behavior (*18*, *19*).

Amygdala function

In higher animals including humans, the amygdala is primarily concerned with the formation and storage of memories associated with emotional events and with emotional influence on behavior. It has been extensively studied in the context of fear memory formation, where it plays a crucial role but has also more recently been linked to social and appetitive behaviors (*18*, *20*, *21*). Human functional magnetic resonance imaging (fMRI) studies show that amygdala activity increases during fear conditioning and that the magnitude of this activity predicts the strength of the conditioned response (*15*) (Fig. 5B). Bilateral amygdala lesions and pharmacological or optogenetic silencing of the amygdala disrupts fear conditioning in rodents, where several lines of evidence indicate that it is essential for the acquisition, storage and expression of fear memories (*20*, *22*).

Amygdalar Microcircuits for fear learning

BLA neurons expressing different genetic markers follow specific connection patterns: PV interneurons preferentially target somata of PNs and SST interneurons, SST interneurons target the dendrites of principal cells and VIP interneurons inhibit other interneurons subtypes, including SST and PV interneurons (Fig. 8) (*23*, *24*).

Under this microcircuit organization, local inhibitory interneurons can exert a powerful control over PN activity. Indeed, optogenetic excitation or suppression of SST or PV neurons activity during fear learning gates the acquisition of fear memories bidirectionally (*24*).

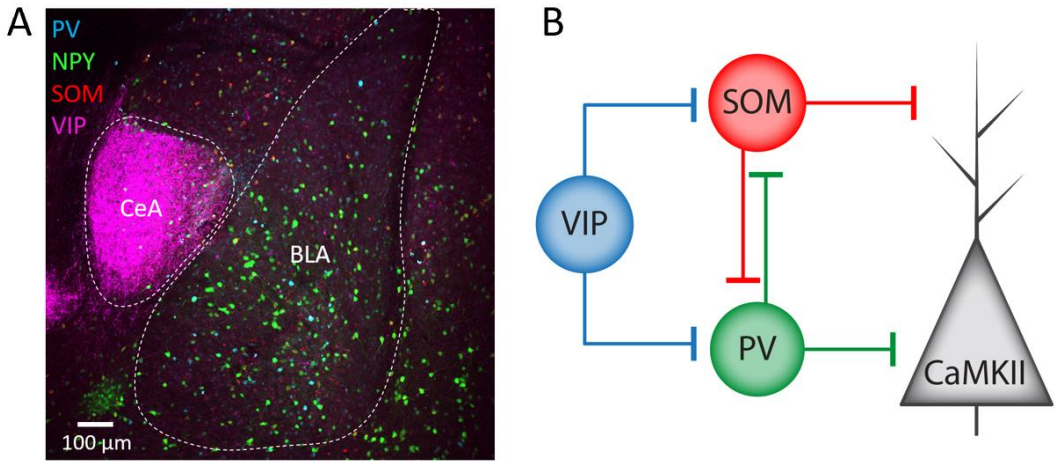


**Fig. 6. BLA neurons subtypes organize in microcircuits.**

**(A)** Immunohistochemistry against the main BLA interneuron cell types. **(B)** Canonical cellular microcircuit In the amygdala: PV interneurons suppress CaMKII neuronal activity by contacting their soma while SST interneurons preferentially target the dendrites. Moreover, SST and PV inhibit each other and are inhibited by VIP interneurons (*24*, *25*).

## Single neuron computations

Long-term plasticity

In the 1970's, the strength of synapses (the physical contact through which neurons are connected) was shown to undergo long-lasting, bidirectional changes termed long-term potentiation (LTP) and long-term depression (LTD) (*26*). Dissection of the molecular pathway underlying this phenomenon revealed that specific patterns of synaptic activity result in $Ca^{2+}$ entry though N-Methyl-D-aspartic acid or N-Methyl-D-aspartate receptors (NMDAR) and α-amino-3-hydroxy-5-methyl-4-isoxazolepropionic acid receptor (AMPAR) into the postsynaptic spine. $Ca^{2+}$ influx in turn leads to the recruitment of CaMKII that ultimately modulates the number of glutamate receptors at the synaptic cleft, and is also accompanied by morphological changes, i.e. spine extension or shrinkage (*27*-*29*)(Fig. 7).

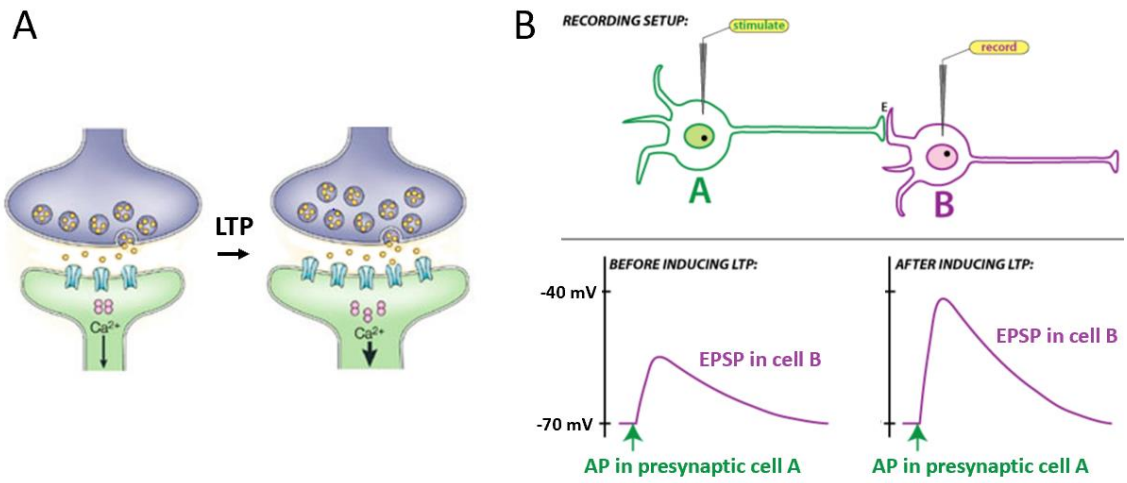


**Fig. 7. Long-term potentiation (LTP) underlies synaptic plasticity.**

**(A)** Upon LTP, additional AMPA vesicles are released at the pre-synapse and additional AMPA receptors are added to the post-synapse. **(B)** LTP results in increased response (Evoked Post-Synaptic Potential) in the post-synaptic neuron upon stimulation of the pre-synaptic neuron. Adapted from (*30*).

This finding established a functional link between pre- and postsynaptic activity and provided a biological substrate to corroborate Donald Hebb's postulate. LTP/LTD has since been identified in various brain regions such as the cerebellum, the hippocampus and the amygdala (*31*–*33*).

In the amygdala, several lines of evidence indicate that LTP underlies the increase in CS response observed after fear learning. Indeed, fear conditioning induces a shift in the AMPAR/NMDAR ratio and prevents further induction of LTP, a mechanism termed LTP occlusion (*34*). In addition, optogenetic or pharmacological blockade prior to fear conditioning via protein synthesis inhibitors or NDMAR blockers disrupt fear learning (*35*, *36*). Some studies also suggest that LTP/LTD of auditory inputs can be induced using *in vivo* using optogenetics (*37*).

In the 1990's, a new plasticity rule termed spike-timing-dependent plasticity (STDP) was discovered. The direction of long-term plasticity of synaptic strength (LTD or LTD) depends on the fine timing between pre- and postsynaptic activity. If the presynaptic activity precedes postsynaptic neuron firing, the result is strengthening of the synapse, but if the presynaptic

follows postsynaptic activity, this results in weakening of the synapse (Fig. 8). This finding has important implications as is shows that neurons can adjust the strength of their connections based on activity causality at a few milliseconds time scale (*38*).

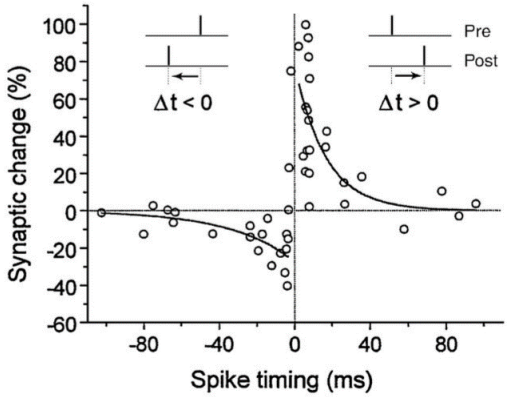


**Fig. 8: Spike timing dependent plasticity.**

When the post-synaptic neuron is repeatedly stimulated before the pre-synaptic neuron ($\Delta t < 0$), the amplitude of the synaptic transmission is reduced. In contrast, when the post-synaptic neuron is repeatedly stimulated after the pre-synaptic neuron ($\Delta t > 0$), the amplitude of the synaptic transmission is increased (*38*).

How the timing of pre- and postsynaptic activity determines the induction of LTP or LTD is not fully understood. However, evidence suggest that upon postsynaptic firing, action potentials can invade the dendritic arbor and further depolarize the previously activated synapses, thereby inducing plasticity. This back-propagation of action potential has been shown to rely on the activation of CaMKII and is believed to play an important role in coincidence detection (*39*, *40*). The role of neuronal activity causally in modulating the strength of synaptic connection provided further support to Hebb's postulate and opened the road to better models to describe how neuronal networks acquire and store new associations and, *in fine*, new memories.

Dendritic integration

Dendrites are branched extensions of neuronal membranes and the main site of synaptic input. Synaptic activation causes cation influx and local membrane depolarization that can propagate to the soma and to the axon initial segment of neurons. There, action potentials are initiated provided the joint subthreshold depolarizations can bring the voltage around the segment to threshold (Fig. 10A, 11). Dendritic activity therefore crucially determines the input-output relationship of neurons.

Dendrites were previously thought to convey electrical stimulation passively, according to passive cable theory (*41*). Under this model, dendritic architecture determines input integration. As a consequence, distal synapse depolarization hardly impacts voltage at the cell body because it gets filtered out through passive electrical diffusion. However, a variety of voltage-gated ion channels present in the membrane of dendrites endow them with active properties (Fig. 9).

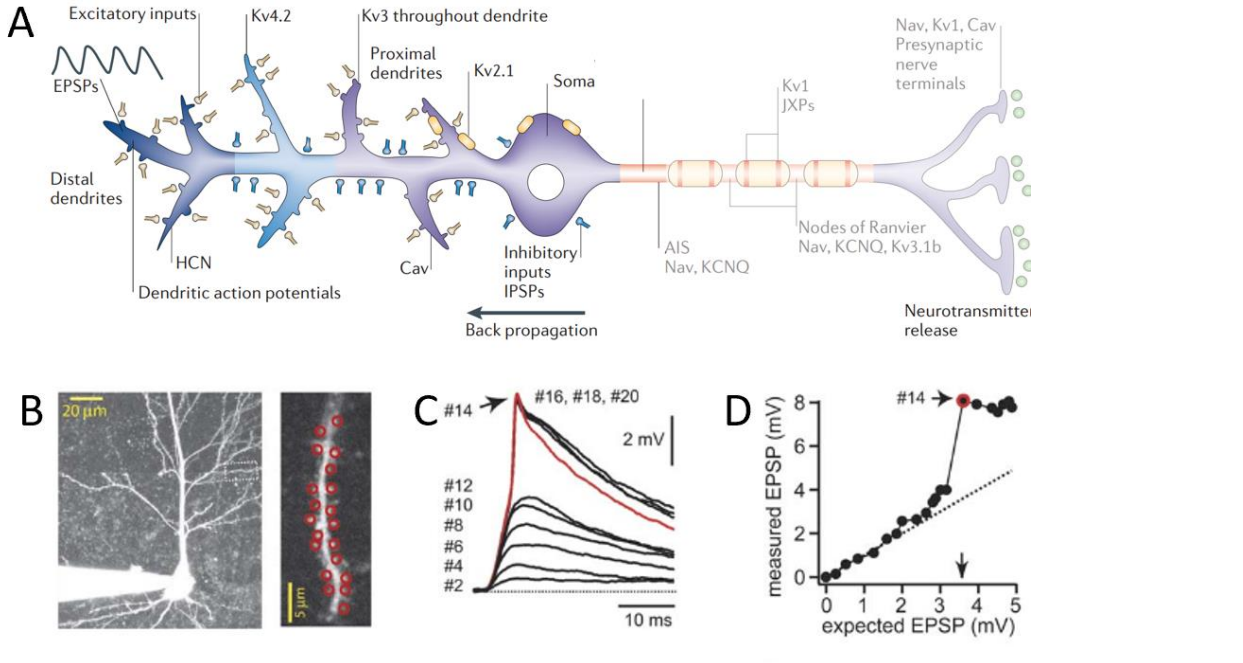


**Fig. 9 Dendritic ion channels allow active integration of synaptic inputs.**

**(A)** Various membrane conductances are located along the dendritic arbor, allowing for non-linear input integration (*42*). **(B)** Somatic voltage recording (left) and location of two-photon glutamate uncaging stimulation (right). **(C-D)** The somatic response to glutamate uncaging is supralinear, meaning greater that the arithmetic sum of individual EPSPs (*43*). HCN : Hyperpolarization-activated Cation Non-Selective, Cav : voltage-gated $Ca^{2+}$ channel ; Kv : voltage-gated $K^{+}$ channel.

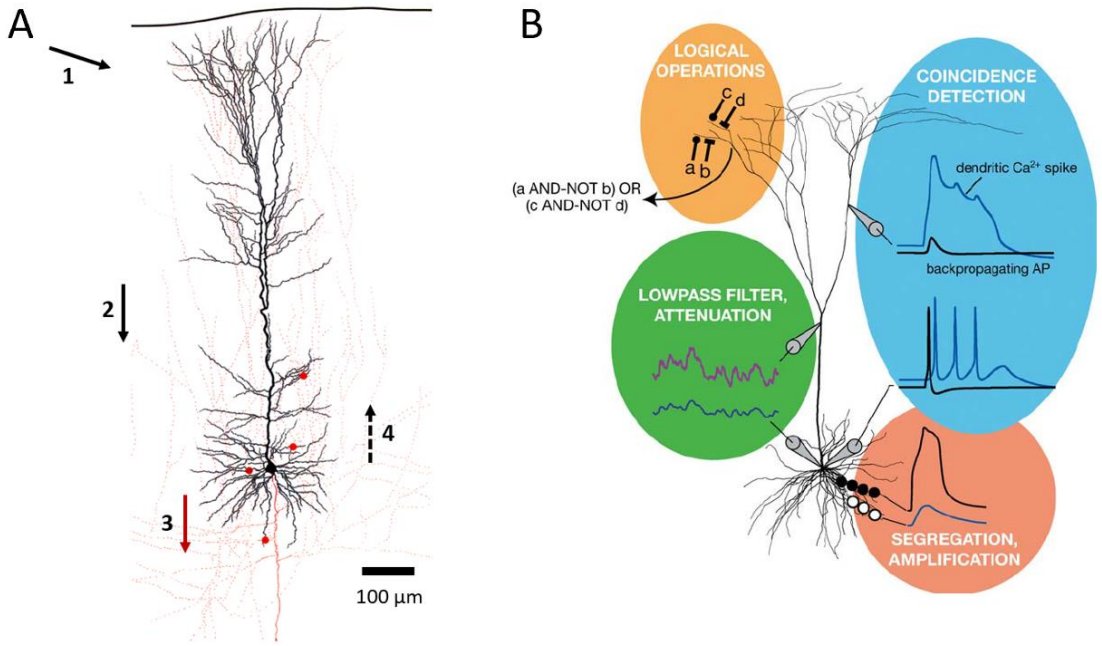


**Fig. 10. Dendritic integration actively shapes neuronal output.**

**(A)** Information flow in a cortical neuron. A cortical pyramidal neuron receives thousands of synaptic inputs, for the most part located in its dendrites (1). Inputs are integrated in the dendritic branches and eventually propagate to the soma (2). If the depolarization threshold is reached, an action potential is generated and propagates along the axon (3). The action potential also propagates back into the dendritic arbor (4). Arrows indicate the direction of information flow (*44*). **(B)** Active and passive properties of dendrites allow single neurons to perform a range of operations. For example, branch-specific activity allows logical operations and backpropagation-activated calcium spikes (BAC) allows coincidence detection (*45*).

Action potential back-propagation

While dendrites propagate membrane depolarization to the cell body, action potentials can also propagate back into the dendritic tree, causing widespread dendritic depolarization and thereby providing individual synapses with the information that the neuron has just fired, which is thought play a role for synaptic plasticity, in particular for STDP (*46*).

Dendritic spikes increase the computational capacity of single neurons

A number of ion conductances allow dendrites to generate their own action potentials, termed dendritic spikes (*47*). Different types of dendritic spikes have been described with different kinetics, spatial spread and involving different ion channels (Fig. 9A). Dendritic

spikes allow dendrites to integrate inputs in a non-linear fashion, which drastically increases the computational power of single neurons (Fig. 9).

*$Ca^{2+}$ imaging in* behaving *animals*

The advent of genetically encoded $Ca^{2+}$ indicators in the 2000's has enabled the recording of activity of entire neuronal populations, providing a wealth of information about neuronal activity patterns during behavior. However, several hurdles still hinder our capacity to comprehend past the mere description of neuronal activity: extracting the general principles and algorithms that underlie higher brain functions such as learning remains a major challenge.

Limitations of cortical imaging

Because of accessibility limitations, imaging large populations of neurons has been largely restricted to cortical areas. Different cortical areas are specialized in processing particular types of information, be it sensory, motor or associating various information streams to carry out higher functions such as decision making. Cortical neuronal representations are complex, typically multidimensional, with single neurons sparsely representing various aspects of sensation and behavior (*48*, *49*). One of the most studied cortical areas is the primary visual cortex (V1). V1 receives well defined inputs from a nucleus only one synaptic relay away from the optic nerve, yet still holds enough complexity to keep researchers busy for many years (*50*). Cortical areas are typically interconnected with a number of thalamic nuclei and other cortices. Such multi-dimensionality of neuronal representation and anatomical interconnectivity are features of the neocortex that make it challenging to decipher what information neural activity actually represents. The behavioral changes that accompany learning, for example, greatly influence neuronal activity, making it problematic to establish causality, *i.e* which aspects of neuronal dynamics are attributable to learning itself and which are reflecting behavior.

Amygdala imaging

A new technology, gradient-index (GRIN) lenses allows the recording of $Ca^{2+}$ activity from populations of neurons in deep brain regions (Fig. 11).

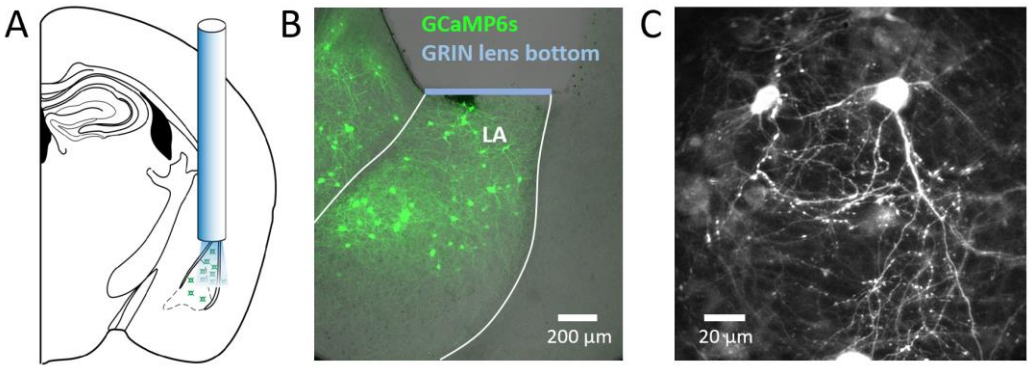


**Fig. 11. Grinded index lens allows deep brain imaging**

**(A)** GRIN lens inplant location scheme. **(B)** Implant location of a fixed brain slice acquired with a confocal microscope. **(C)** Fine subcellular structural details can be resolved *in vivo* with two-photon microscopy, here labelled with GCaMP6s.

The amygdala is intimately linked to the formation, storage and expression of emotional memories and contains populations of neurons with stable sensory representations (*18*). The first longitudinal amygdala imaging experiment was performed by Grewe et al. in 2017 (*51*). In this study, the authors tracked the activity of BLA PN across a fear conditioning paradigm. At the population level, fear conditioning induced a stable shift in the CS representation, which became more similar to the US representation, suggesting that during fear conditioning the CS representation acquires some properties of the innately aversive US. Moreover, much of the observed CS representation shift took place overnight when memory consolidation is thought to occur (*52*). The authors observed neurons that increase their CS response during conditioning (CSup neurons) but also a population of neurons that decrease their CS response during learning (CSdown). Importantly, both neuronal populations contributed to encoding the shift in CS representation towards the US representation.

Hebbian learning predicts that neurons that respond to the US are more likely to increase their CS response after fear conditioning. However, this study found no correlation between the direction of CS response change and the US responsiveness of BLA PNs. Moreover, Hebbian learning fails to account for the observation of CSdown neurons. Together, these discrepancies argue against purely Hebbian learning during fear conditioning. However,

since $Ca^{2+}$ imaging was restricted to the somata of BLA PNs, the question remains whether activity in the dendrites of these neurons could differ from that observed in somata and could help elucidate some of the discrepancies.

Dendritic $Ca^{2+}$ imaging

$Ca^{2+}$ activity in dendrites can be recorded using fluorescent indicators like GCaMP combined with two-photon microscopy, provided sparse neuronal labelling. This approach has been used to image the PNs dendrites from different layers across the cortex during behavior (*53-55*). A subset of these studies performed simultaneous somatic and dendritic imaging and confirmed that dendritic activity could be restricted to individual branches, but that in many cases $Ca^{2+}$ activity was shared between soma and dendrites in the form of global events, likely involving back-propagating action potentials (bAPs). However, simultaneous imaging of somatic and dendritic activity from deep-brain areas has not yet been performed.

The ability to track activity across days in different neuronal compartments of single neurons over the course of learning offers the possibility to better understand how memory formation affects the integration of sensory cues and whether localized plastic changes occur in dendrites.

# Aim of the thesis

There is ample evidence that principal neurons in the lateral amygdala undergo synaptic plasticity of auditory inputs during classical fear conditioning and that these plastic changes underlie the formation of an associative memory that binds CS and US. The vast majority of synaptic inputs contact the dendrites of these neurons, yet how the inputs conveying the CS and US information are integrated by single neurons is unknown. Furthermore, the coupling between dendritic and somatic activity is highly regulated. The relative dendritic and somatic $Ca^{2+}$ activity has been studied in the neocortex, in the hippocampus and in the cerebellum, but little is known about somato-dendritic coupling in deep brain regions such as the amygdala. The aim of my thesis was twofold: on one hand, I wanted to study how sensory stimuli are represented in principal neurons in the lateral amygdala dendrites and somata *in vivo*. To this end, I characterized dendritic and somatic $Ca^{2+}$ activity in single neurons during and outside sensory stimulus presentations. I then asked how associative learning modifies dendritic activity and the relationship between somatic and dendritic plasticity of conditioned stimulus responses, as we hypothesized could result from the synaptic changes occurring during fear conditioning.

# Materials and methods

## Animals

All animal procedures were performed in accordance with institutional guidelines at the Friedrich Miescher Institute for Biomedical Research and were approved by the Veterinary Department of the Canton of Basel-Stadt. SST-ires-Cre mice (*56*) were used for Cre-dependent expression of viral vectors. Only heterozygous (Cre/ wild-type) mice were used for experiments and were backcrossed to a C57BL/6J background for more than ten generations. For all other experiments, male wild-type C57BL/6J mice (Envigo, the Netherlands) aged 2–3 months at the time of virus injection were used. Mice were individually housed for at least 14 days before starting behavioral paradigms. Animals were kept in a 12 h light–dark cycle with access to food and water ad libitum as well as a shelter and a running wheel. All behavioral experiments were conducted during the light cycle.

## Surgical procedure

We performed surgeries when mice were 9–10 weeks of age. Mice were anesthetized using isoflurane (3–5% for induction, 1–2% for maintenance; Attane, Provet) in 95% O2 (Praxair) and fixed on a stereotactic frame (Kopf Instruments). Injections of buprenorphine (Temgesic, Indivior UK Limited; 0.1 mg per kg body weight subcutaneously 30 min before anesthesia) and ropivacain (Naropin, AstraZeneca; 0.1 ml locally under the scalp before incision) were provided for analgesia. Postoperative pain medication included buprenorphine (0.1 mg per kg in the drinking water; overnight) and injections of meloxicam (Metacam, Boehringer Ingelheim; 1 mg per kg subcutaneously) for up to 3 days if necessary. Ophthalmic ointment was applied to avoid eye drying. The body temperature of the experimental animal was maintained at 36°C using a feedback- controlled heating pad (FHC).

For the imaging of somata and dendrites, mice were injected with an AAV2/9-CamKII-Cre-SV40 diluted in sterile saline (final dilution 1:20000) mixed 1:1 with AAV2/1-hSyn-flex-GCaMP6s (final dilution: 1:2), resulting in sparse labelling of LA PNs. For combined imaging and chemogenetic manipulations of SST interneurons, SST-ires-Cre mice were injected with an AAV2/1-CamKII-FLPo diluted in sterile saline (final dilution 1:5000) mixed 1:1:1 with AAV2/1-Ef1a-fDIO-GCaMP6s (final dilution 1:3) and AAV2/1-hSyn-DIO-hM4D(Gi)-mCherry

(final dilution 1:3). The virus mix (approx. 300 nl) was unilaterally injected into the BLA using a precision micropositioner (Model 2650, Kopf Instruments) and pulled glass pipettes connected to a Picospritzer III microinjection system (Parker Hannifin Corporation) at the following coordinates from bregma: AP: –1.55 mm; ML: –3.4 mm; DV: –3.75 to –4.15 mm. During the same surgery, a GRIN microendoscope (GRIN lens, 0.6 × 7.3 mm, GLP-0673, Inscopix) was implanted into the LA as previously described (*57*). In brief, a sterile needle was used to make an incision above the imaging site. The GRIN lens was subsequently lowered into the brain using a micropositioner (coordinates from bregma: AP: –1.55 mm; ML: –3.4 mm; DV: 4.0 mm) with a custom-built lens holder and fixed to the skull using ultraviolet light-curable glue (Henkel, Loctite 4305). A mix of dental acrylic (Paladur, Heraeus) and black acrylic paint was used to seal the skull and attach a custom-made head bar for animal fixation during imaging experiments. Mice were allowed to recover for at least 14 days after GRIN lens implantation before checking for GCaMP expression.

## Two-photon imaging

2-4 weeks after surgery, mice were head-fixed on a running wheel to check for sufficient expression of GCaMP6s under a two-photon microscope (Ultima Investigator, Bruker, USA). When sufficient expression levels were reached (5-10 weeks after surgery), mice were habituated to a brief head-fixation under the microscope while free to run on a wheel for at least 2 days before any behavioral paradigm. GCaMP6s signals were recorded at a 30 Hz from a field of view of 370 x 370 µm (512 x 512 pixels) through a water immersion objective (25x, 1.05 numerical aperture (NA), Olympus). Ultrasound gel (G008, FIAB spA) was used to interface the objective and the GRIN lens. Excitation light was provided with a mode-locked laser system operating at 920 nm, 80-MHz pulse repeat, < 120-fs pulse width (Insight X3, Spectra Physics, Mountain View, CA). For simultaneous imaging of GCaMP6s and tdTomato, excitation light was provided at 960 nm instead and green and red emission light was filtered through specific bandpass filters (green emission light: 525/70m; red emission light: 595/50m, both Chroma Technology) and detected by different PMTs (photomultipliers, Hamamatsu Photonics). For individual mice, the same imaging parameters were kept across repeated behavioral sessions. Imaging data were recorded using Prairie View Software (Bruker, USA). For detailed structural scan acquisition, mice were injected IP with FMM

(Fentanyl-Curamed, 0.05 mg per kg of body weight, Midazolam, 5 mg per kg of body weight, Medetomidine, 0.5 mg per kg of body weight). Ophthalmic ointment was applied to avoid eye drying. The body temperature of the experimental animal was maintained at 36 °C using a feedback- controlled heating pad (FHC). An imaging volume, centered on the imaging plane previously used for functional imaging, was acquired with a 2 µm increment between each plane. Each image was obtained by averaging 128 frames from a field of view of 471 x 471 µm (1024 x 1024 pixels). The dendritic arbors of the imaged neurons were tracked in 3-D using the simple neurite tracer plugin in ImageJ (*58*) and mapped onto the corresponding functional imaging data. This allowed associating functionally imaged dendritic branches with their parent soma.

## Mouse behavior

To assess tone and shock tuning and stability, mice were head-fixed on a running wheel under a two-photon microscope. A rotary encoder (SparkFun Electronics) was used to record running speed. On each session, mice were allowed to habituate to the setup under head fixation for at least 15 min prior to the start of any experimental paradigm. For auditory stimulus delivery, an electrostatic speaker (ES1, Tucker-Davis Technologies) was placed on each side of the mouse head. 3 s continuous pure tones (75-85 dB, 3-18 kHz) were generated using a System 3 RP2.1 real-time processor and a SA1 stereo amplifier with RPvdsEx Software (all Tucker-Davis Technologies). On two consecutive days, tones were presented in a random order of frequencies and with increasing sound pressure levels on 2 consecutive days with an inter-trial interval (ITI) of 90 s. In a subset of mice, the same tone presentation protocol was applied for 4 consecutive days. For electrical shock delivery, a small two pin connector (Fischer Elektronik) was brought in contact to the forehead of the mouse, between the eyes and the ears, and connected to a precision animal shocker delivering direct current (DC). On the last day, 20-30 min after the last tone presentation, 1 s electrical shocks with increasing intensities (0.1-0.65 mA) were delivered with an inter-trial interval (ITI) of 120 s. Behavioral protocols for stimulus control were generated using the Prairie View Software (Bruker, USA) via TTL (transistor-to-transistor logic) pulses. For chemogenetic inhibition of SST interneurons, mice were injected IP (intraperitoneally) with saline (0.9 % NaCl) on day

1 and with CNO (5 mg per kg, Tocris) on day 2. Tones were presented on both days following the same presentation protocol as described in this section.

## Fear conditioning paradigm

On day 1, mice were habituated to two different pure tones (CS: 7 kHz and 12 kHz, 3 s; 80 dB sound pressure level) presented 10 times in an alternating fashion with a 120 s inter-trial interval (ITI). On day 2, mice were conditioned to one of the pure tones (CS+) by pairing it with a US (1 s electrical shock, 1 mA) delivered as described in the previous section. The US was applied directly after the CS+. The other pure tone was used as a CS– and was not followed by a US. CS+ with US and CS– were presented 10 times each in an alternating fashion with a 120 s inter-trial interval (ITI). In a separate group of mice that underwent pseudo-conditioning, the US was applied at least 120 s apart from any CS. On day 3, similar to day 1, two different pure tones (CS: 7 kHz and 12 kHz, 3 s; 80 dB sound pressure level) were presented 10 times in an alternating fashion with a 120 s inter-trial interval (ITI). On each day, the use of 7 kHz and 12 kHz as CS+ was counterbalanced within individual groups.

## Freely moving behavior

In parallel with head-fixed fear conditioning under a two-photon microscope, fear memory was tested in freely moving conditions in the same animals. On day 1 and day 3, mice were placed in a circular arena with Plexiglas walls in a sound-isolated box. After a 2 min baseline period, 3 CS– followed by 3 CS+ (30 s, continuous pure tone, 80 dB sound pressure level) were presented with a 90-120 s pseudorandom inter-trial interval (ITI). Freezing responses were quantified on day 1 (habituation) and day 3 (test) during stimulus presentation (CS: 30 s continuous pure tone, 7 and 12 kHz). Behavioral protocols for stimulus control were generated using Radiant software (Plexon) via TTL (transistor-to- transistor logic) pulses. The animal motion was tracked during the CS period and freezing during the CS+ presentations on day 1 and day 3 was compared to evaluate associative learning.

## Dendritic arbor reconstruction

Following any behavioral paradigm, mice were hosted for an additional 4-6 weeks to allow for maximal GCaMP6s expression. Then, mice were anesthetized with FMM (*59*) and placed under a two-photon microscope. A detailed depth scan was acquired around the plane

imaged during behavior. During this procedure, ophthalmic ointment was applied to avoid eye drying. The body temperature of the experimental animal was maintained at 36 °C using a feedback- controlled heating pad (FHC). The dendritic tree of previously imaged neurons were reconstructed post-hoc from the 3-D structural scan with simple neurite tracer plugin, ImageJ (*58*). Overlay with the functional imaging data allowed associating imaged dendritic branches with their parent somata.

## Analysis of calcium imaging data

Basic image pre-processing: briefly, for each imaging session, recordings from all trials were concatenated into an image stack, corrected for bidirectional scanning (*60*), down sampled spatially by 2 x 2 pixels, and background was subtracted. Then, images were corrected for rigid and for non-rigid motion using Normcorre (*60*). Registration across imaging sessions: after pre-processing as described, the mean intensity projections of each imaging session were registered using imregister in Matlab (MathWorks) and the resulting shifts applied to all single frames. To check that GCaMP signal alone is sufficient for appropriate motion registration of subcellular compartments, we conducted a control experiment to compare image registration using either GCaMP or the $Ca^{2+}$ insensitive fluorescent marker tdTomato as reference (Fig. 14).

For selecting subcellular compartments, non-overlapping somata, dendritic branches and dendritic spines were selected manually as regions of interest (ROIs) in ImageJ using the ROI manager tool. The mean fluorescence intensity of all pixels from each ROI was considered for further analysis. Relative changes in $Ca^{2+}$ fluorescence (F) were calculated using the formula: $\Delta F/F0 = (F - F0)/F0$ (with F0 = mean fluorescence of entire trace) and used for all analysis of $Ca^{2+}$ activity. All analysis was conducted in Matlab.

## Data analysis

To identify responsive subcellular compartments, average $Ca^{2+}$ traces were compared between the stimulus presentation period and a baseline period of the same duration. The stimulus response period was set to 3 s for shock presentations. For fear conditioning, US responsiveness was assessed by using the last second of CS presentation as baseline instead. If the mean $Ca^{2+}$ activity during the stimulus period was larger or smaller than the mean $Ca^{2+}$

activity during the baseline period by more than 2 SD (standard deviations), the ROI was classified as responsive (excited or inhibited, depending on response sign). Otherwise, the ROI was classified as unresponsive. To identify functional sub-classes of neurons, we classified neurons in four mutually exclusive categories based on their CS responses on day 1 (habituation) and day 3 (test) as follows: (1) CS unresponsive: CS unresponsive on day 1 and day 3; (2) CS neutral: same CS response identity (positive or negative response) on day 1 and on day 3 and absolute difference between the CS responses on day 1 and day 3 smaller than 15 % ΔF/F0; (3) CSup: CS response on day 3 larger than on day 1, excluding CS unresponsive and CS neutral neurons; (4) CSdown: CS response on day 3 smaller than on day 1, excluding CS unresponsive and CS neutral neurons. For intra session CS response amplitude comparison, responses to the first and the last CS presentation on each session were compared.

## Probability and amplitude of stimulus response

To assess response probability, $Ca^{2+}$ activity was compared between the stimulus presentation period and a baseline period of the same duration. The stimulus response period was set to 3 s for shock presentations. Response probability was defined as the proportion of trials where the mean $Ca^{2+}$ activity during the stimulus period was larger than 2 standard deviations (SD) of the $Ca^{2+}$ activity during the baseline period. Response amplitude was calculated from the average of all responsive trials. To compare the probability of response between days, the ratio of response probability was computed for each compartment. To compare the amplitude of response between days, the difference of response amplitude was computed for each compartment.

## Calcium transient detection and normalization

$Ca^{2+}$ transients were detected in somata, dendritic branches and dendritic spines using the findpeaks Matlab function with the following criteria: ΔF/F0 exceeding 1 SD (standard deviation) of the entire trace, prominence exceeding 0.5 SD (standard deviation) of the entire trace. Within single neurons, $Ca^{2+}$ transients in the dendrites and soma were defined as co-occurring when their peak amplitude was detected within a time window of 2 s, in order to account for the variability of the $Ca^{2+}$ indicator rise time in different compartments. $Ca^{2+}$ transients detected during the tone presentation period were defined as tone-locked, $Ca^{2+}$

transients detected outside of the tone presentation period as spontaneous. To compare the amplitude of $Ca^{2+}$ transients in the soma and in dendritic branches, the $Ca^{2+}$ trace of each compartment was normalized to its maximum ΔF/F0.

## Histology

Following completion of any behavioral paradigm, mice were transcardially perfused. Brains were post-fixed in 4% paraformaldehyde for at least 2 h at 4 °C and cut into 100 µm coronal slices using a vibratome (VT1000S). Sections containing the amygdala were immediately mounted on glass slides and coverslipped. To verify the GRIN lens implantation site, sections were scanned with a 10× air objective (Plan-Apochromat 10×/0.45) using a laser scanning confocal microscope (LSM700). GRIN lens placements were matched against a mouse brain atlas (*61*).

## Statistical analyses and data presentation

Statistical analyses were carried out using Matlab (MathWorks). The sample sizes are similar to those used in the field. No statistical methods were used to determine sample size. Animals were post hoc excluded from the analysis in the following three cases: (1) the bottom tip of the GRIN lens was located outside the LA; (2) brain motion was too great to be corrected post-hoc; (3) GCaMP6 labelling was not sparse enough to allow isolation of dendritic signals. The following number of mice were rejected, given for each per cohort: sensory stimuli tuning and stability: N = 1; Fear conditioning: N = 4; Pseudo-conditioning: N = 3 mice. All datasets were tested for Gaussian distribution using a Kolmogorov–Smirnov normality test. Datasets were compared using a Student's t-test if the null hypothesis of normal distribution was not rejected. One-way ANOVA tests were used when comparing more than two normally distributed datasets. Post hoc multiple comparisons were performed using the Bonferroni correction. If the null hypothesis of normal distribution was rejected, two datasets were compared using Wilcoxon signed-rank test. Two-sample Kolmogorov-Smirnov tests were used to evaluate the difference of two samples probability distributions. A Chi-square test of proportions as conducted to compare proportions between two groups. A statistical significance threshold was set at 0.05, and significance levels are presented as *P < 0.05, **P < 0.01 or ***P < 0.001 in all figures. Averaging across multiple trials is indicated in the figure legends and respective methods sections where applicable. Contrast and brightness of

representative example images were minimally adjusted using ImageJ or Zen lite Software (ZEISS technology). For figure display, $Ca^{2+}$ traces were presented as ΔF/F0 or z-score (z = (F – F0) / σ, with F0 = mean fluorescence and σ = standard deviation over the entire $Ca^{2+}$ traces).

# Results

## Deep brain imaging of lateral amygdala neurons somata and dendrites

We virally expressed a Cre-dependent version of the $Ca^{2+}$ sensor GCaMP6s together with highly diluted AAV2/1-CaMKII-Cre (Fig. 12A, see methods) and implanted a gradient- index (GRIN) lens above the virus injection site in the LA (Fig. 13) to monitor somatic and dendritic activity in LA PNs. This approach resulted in sparse GCaMP expression in LA PNs and minimal background fluorescence from out of focus sources when imaged though with a two-photon microscope (Fig. 12C,E-F). Somata and dendrites could be identified across multiple imaging sessions, allowing us to reliably track activity across days (Fig. 12D-E). Importantly, $Ca^{2+}$ imaging movies could be registered accurately based on CGaMP6s expression alone and did not require the use of an additional $Ca^{2+}$-independent structural marker (Fig. 14). Unlike neocortex, the amygdala is not organized in layers, making it challenging to associate dendrites with their parent soma. To solve this issue, we reconstructed the dendritic arbors of imaged neurons around the imaging plane based on a detailed structural scan acquired though the GRIN lens after the completion of the behavioral experiments, in anesthetized animals (Fig. 12G).

Auditory stimuli and mild electrical shocks are commonly used as the conditioned stimulus (CS) and unconditioned stimulus (US) respectively to study associative fear learning. However, it is unclear how these modalities are represented in different subcellular compartments of LA PNs. Our approach allows simultaneous somatic and dendritic recordings of CS and US responses of LA PNs in awake mice (Fig. 15).

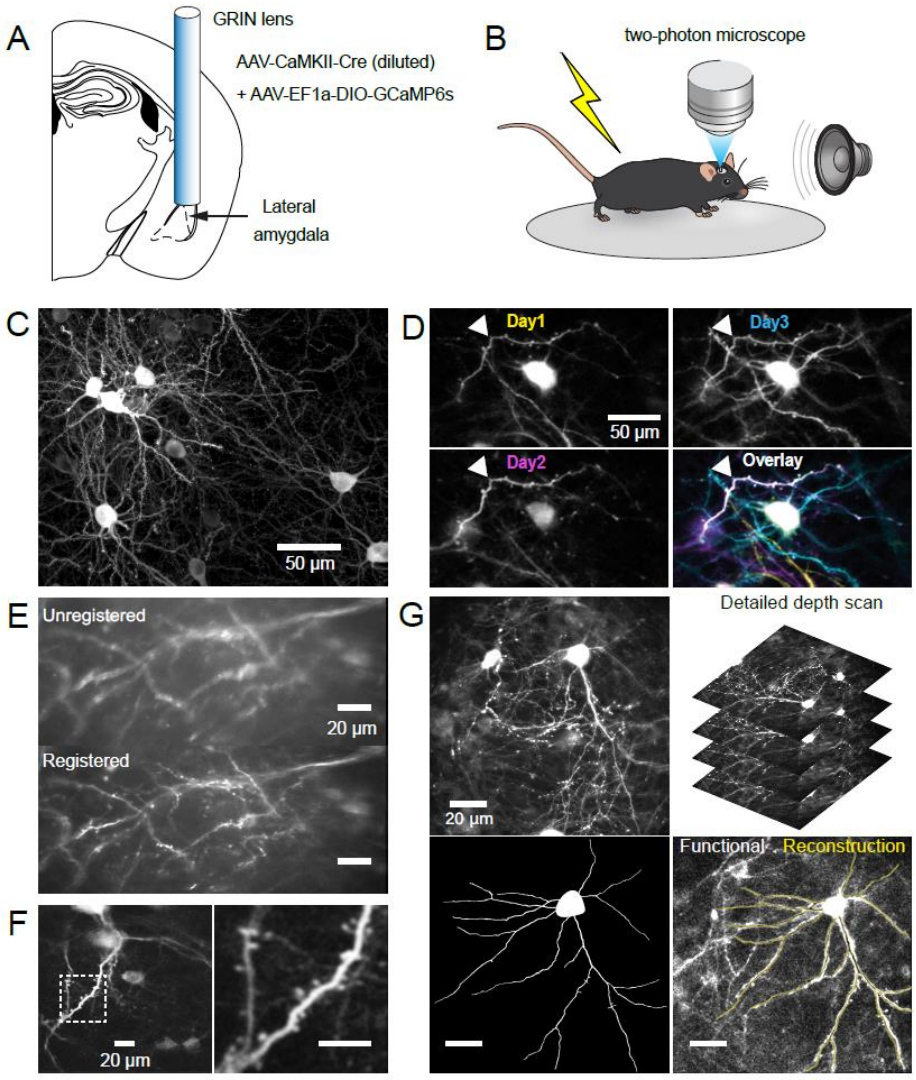


## Fig. 12. In vivo dendritic $Ca^{2+}$ imaging in the lateral amygdala.

**(A)** Left: injection of a highly diluted viral vector encoding CaMKII-Cre allows for sparse but robust expression of GCaMP6s in LA PNs. A GRIN lens is implanted to gain optical access to the LA. **(B)** Head-fixed mice are allowed to run freely on a wheel under a two-photon microscope while presented with tone and shock stimuli. **(C)** Confocal image of LA PNs neurons sparsely expressing GCaMP in the LA. **(D)** Imaging plane relocation in an awake mouse over three consecutive days. Each image was obtained by averaging 50 imaging frames recorded at 30 Hz. The white arrow indicates the same dendritic segment active over days. Bottom right: overlay of the three days, one color per day. **(E)** Different steps of image registration. Each picture shows an average over the same 1000 frames recorded at 30 Hz. A combination of full frame and piece-wise rigid registration with NormCorre (*60*) allows to register fine subcellular compartments. **(F)** Partial reconstruction of the dendritic arbor of imaged neurons. The dendrites of the imaged neurons were tracked in 3-D based on a structural scan

acquired under anesthesia after the experiment (bottom left) and mapped back onto the functional imaging data (bottom right).

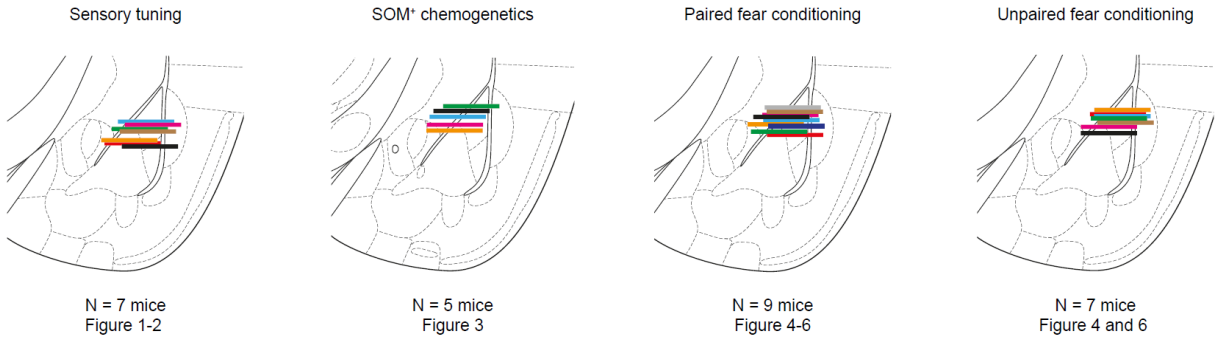


## Fig. 13. GRIN lens implantation locations.

For each experimental group, the location of the bottom of the GRIN lens for each mouse is represented by a line and mapped onto a mouse brain atlas (-1.72 mm posterior to lambda (*61*)).

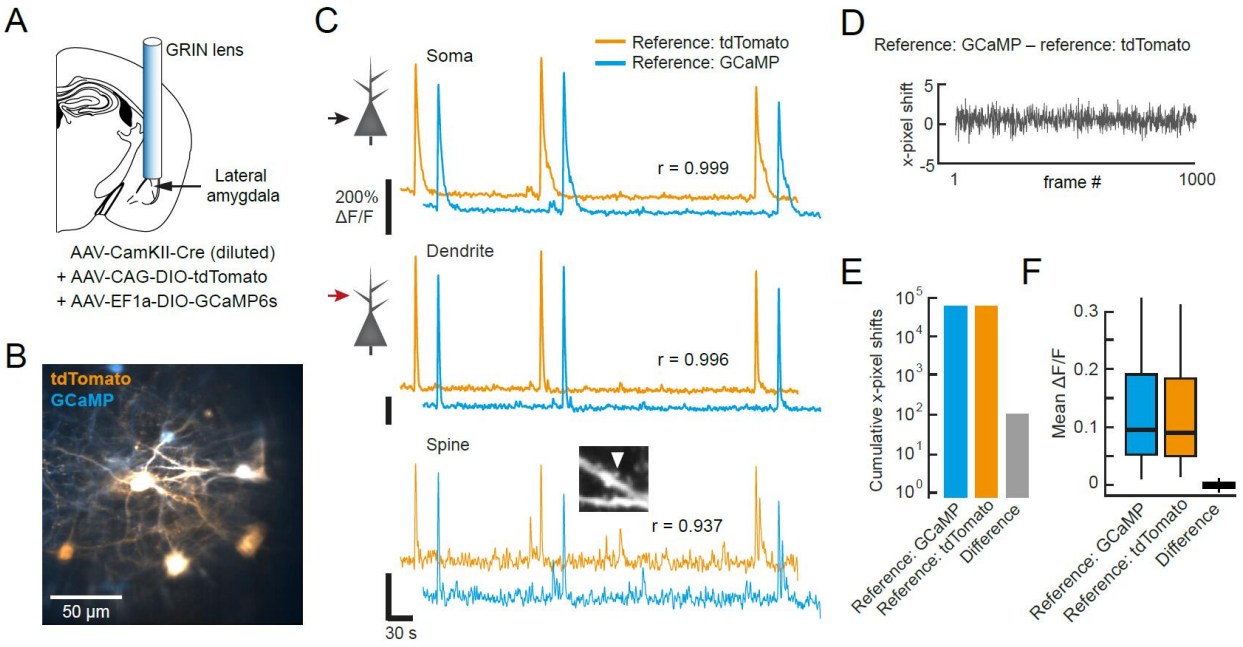


## Fig. 14. Similar performance using GCaMP or TdTomato as reference for image registration.

**(A)** Viral strategy for sparse expression of GCaMP and tdTomato**. (B)** Mean intensity projection though a GRIN lens after image registration using GCaMP6s as a reference. **(C)** Similar $Ca^{2+}$ activity traces are obtained using GCaMP6s or tdTomato as image registration references. Correlation between example soma, a dendrite, and a dendritic spine. $Ca^{2+}$ traces obtained after registration using GCaMP6s or tdTomato as a reference, and overlap between traces (*r*, Pearson's correlation). **(D)** Minimal frame-by-frame x-pixel shift difference between

registration using GCaMP6s or tdTomato as reference. Pixel size = 0.62 µm2. **(E)** Minimal summed absolute shifts difference between registration using GCaMP6s or tdTomato as reference. Data are shown in log scale. **(F)** Minimal mean ΔF/F0 difference between registration using GCaMP6s or tdTomato as reference (n = 23 subcellular compartments). Box-and-whisker plots show median values and 25th and 75th percentiles, the maximum whiskers length is 1.5 times the interquartile range.

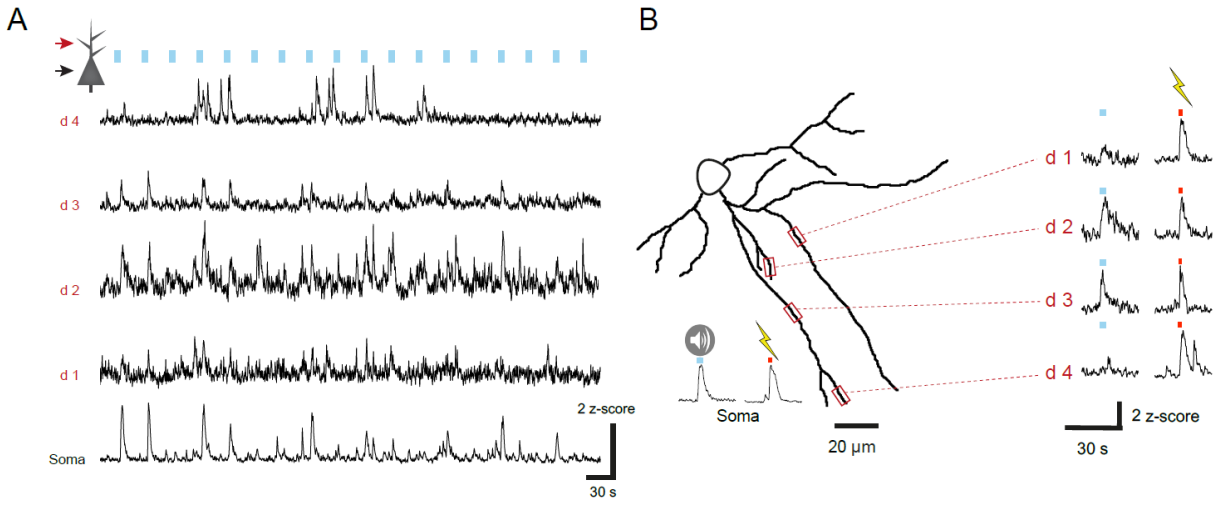


**Fig. 15. Simultaneous imaging of somatic and dendritic tone and shock responses.**

**(A)** Simultaneous $Ca^{2+}$ imaging in the soma and dendrites of a LA PN neuron in (G). Blue rectangles indicate tone presentations. **(B)** Reconstruction of part of a LA PN neuron dendritic tree. Awake mice are presented with mild aversive electrical shocks and pure tones, allowing to investigate somatic and dendritic responses in the soma and dendrite of the same neurons.

## $Ca^{2+}$ activity coupling between LA PN somata and dendrites

We detected $Ca^{2+}$ events (see Methods) in identified dendritic branches of single neurons and compared them to somatic transients to investigate the extent of functional coupling between the soma and dendrites of the same cell (Fig. 16A-C). We found that the amplitude of simultaneous somatic and dendritic events was correlated but that the strength of this correlation decreased with increasing distances from the soma (Fig. 16D-E), indicating that activity in distal dendrites is more decorrelated from the soma. Moreover, spontaneous dendritic $Ca^{2+}$ events had a smaller relative amplitude when compared to their parent somata (Fig. 17A). It is plausible that many of these dendritic transients originate from back-

propagating action potentials (bAP) (see Discussion). Consistent with this notion, the majority of dendritic $Ca^{2+}$ events were accompanied by $Ca^{2+}$ transients at the soma (Fig. 17B).

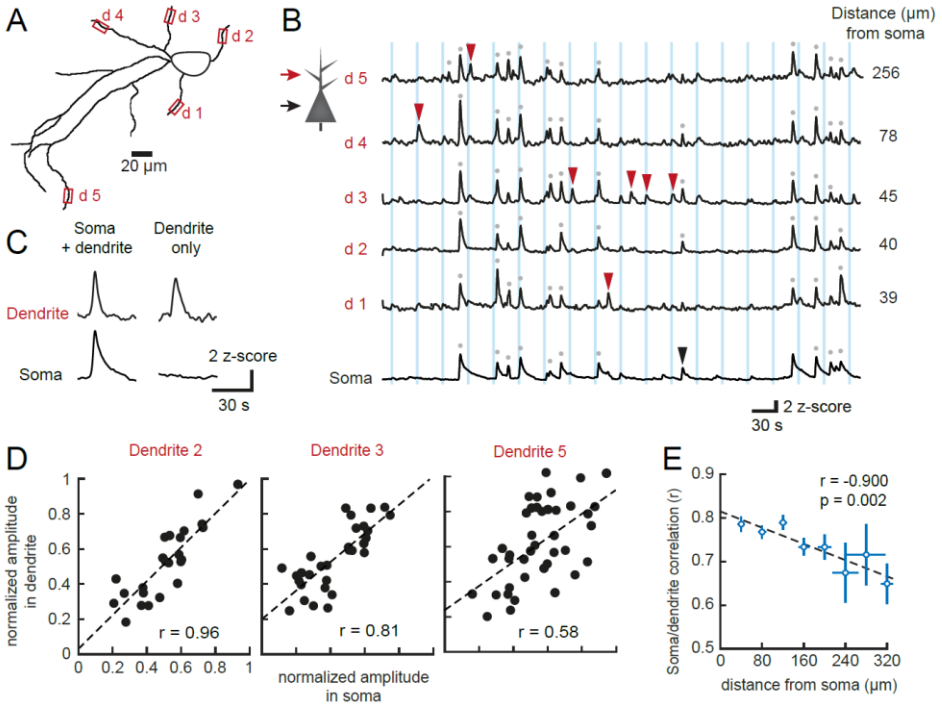


**Fig. 16. Variability of soma-dendrite coupling in single neurons.**

**(A)** Reconstructed dendritic arbor of a recorded neuron. **(B)** $Ca^{2+}$ traces of the soma and five dendritic branches of the same neuron. The numbers indicate the location of the dendritic segments shown in (A). Blue vertical lines indicate tone presentations, gray dots: detected $Ca^{2+}$ transients, arrowheads: compartment-specific $Ca^{2+}$ transients. **(C)** Example of automatically detected $Ca^{2+}$ events classified as "soma + dendrite" or "dendrite only". **(D)** Soma-dendrite coupling is heterogenous. Normalized $Ca^{2+}$ transient amplitude correlation between the soma and dendrites in (A) (*r*, Pearson's correlation). **(E)** Soma-dendrite coupling decreases with distance from the soma. *r*, Pearson's correlation between somatic and dendritic $Ca^{2+}$ traces. Data are binned according to distance from soma (mean ± SEM, 113 soma-dendrite pairs from 13 neurons).

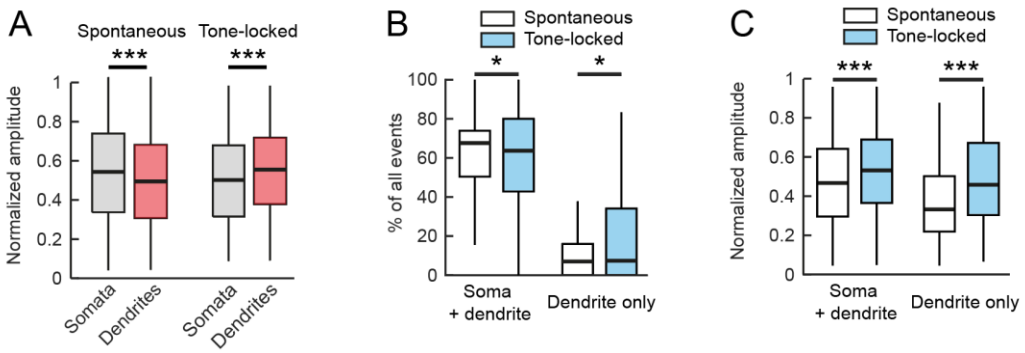

**Fig. 17. Increased dendrite-specific activity during tone.**

**(A)** Normalized $Ca^{2+}$ transients amplitude in somata and dendrites during spontaneous and tone periods (spontaneous: $p < 0.001$ , n = 7969 transients from 113 soma-dendrite pairs; tone-locked: $p < 0.001$ , 1961 tone-locked transients, both Wilcoxon signed-rank test). **(B)** Higher proportion of dendrite-specific transients during tone (soma + dendrite, p = 0.010, dendrite only, p = 0.029, both Wilcoxon signed-rank test, n = 11212 spontaneous and 2147 tone-locked transients from 113 soma-dendrite pairs from 13 neurons). **(C)** Dendritic $Ca^{2+}$ transients have a larger amplitude during tone presentation than during spontaneous activity. Normalized $Ca^{2+}$ amplitude of dendrite only and dendrite + soma transients during spontaneous and tone-locked periods (both $p < 0.001$, Wilcoxon signed-rank test, n = 1388 spontaneous and 354 tone-locked transients from 113 soma-dendrite pairs from 13 neurons). Box-and-whisker plots show median values and $25^{th}$ and $75^{th}$ percentiles, the maximum whiskers length is 1.5 times the interquartile range.

We asked whether sensory tuning could differ in LA PNs somata and dendrites and presented mice with different tone frequencies and intensities and with different intensities of electrical shocks (Fig. 18A). Different somata and dendrites of LA PNs harbor diverse tuning to tones and shocks, potentially allowing for highly specific CS-US associations. However, dendrites of single neurons had similar tuning as their parent soma (Fig. 18E-G). One possible explanation for why dendrite-specific sensory tuning was not observed could be that bAP typically have a larger amplitude than dendritic spikes and therefore dominate the average $Ca^{2+}$ response to sensory stimulus.

In the neocortex, recent studies suggest that activity in dendritic branches and their parent soma is strongly correlated (*55*, *62*, *63*). In this dataset, ca. 10 % of dendritic $Ca^{2+}$ events in LA PNs were exclusive to specific dendritic branches (Fig. 17B) and not coincident with somatic events, indeed suggesting strong functional coupling between LA somata and dendrites during spontaneous activity.

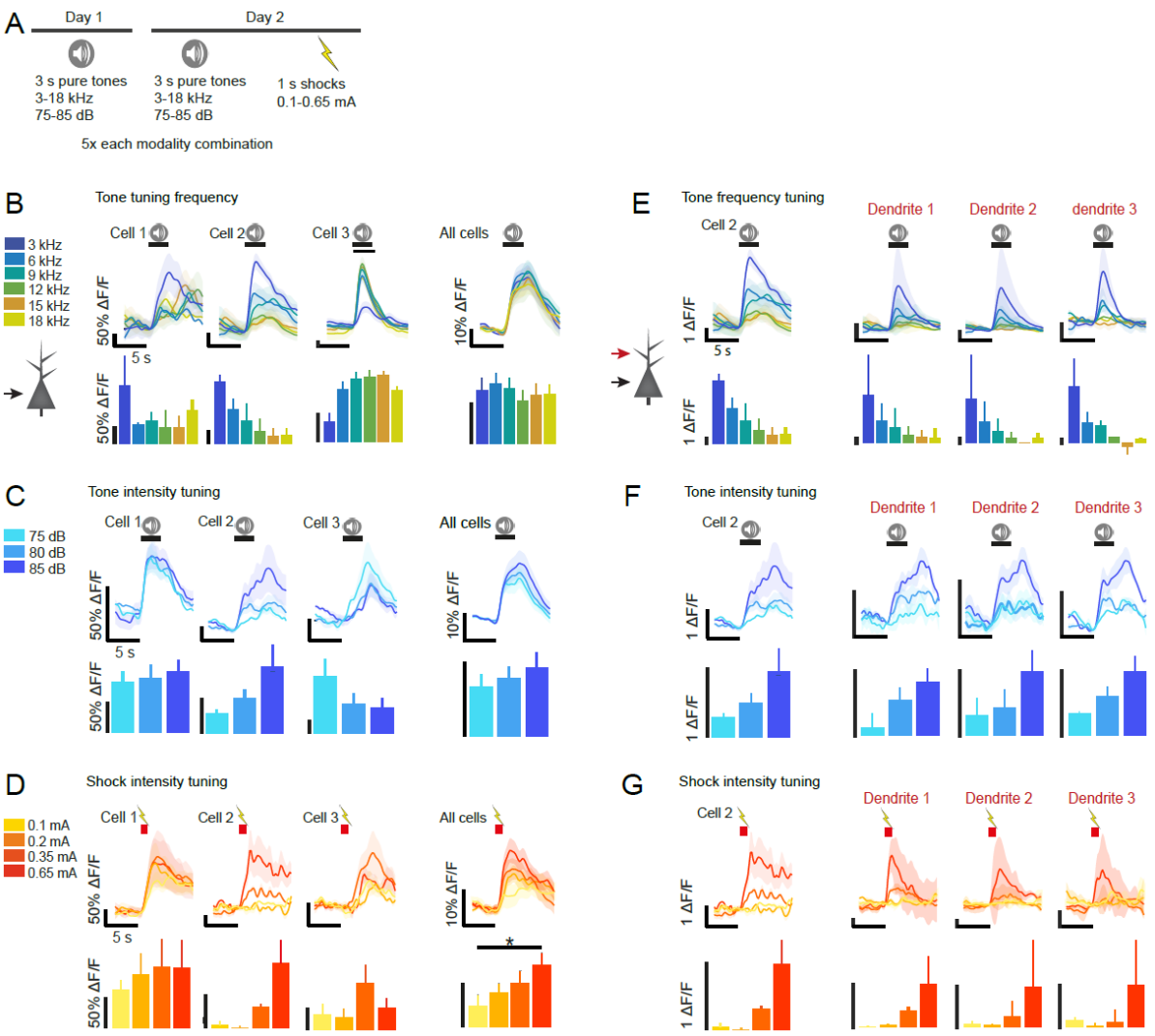


**Fig. 18. Sensory mapping of LA PNs somata and dendrites.**

**(A)** Sensory mapping protocol. Naïve mice were presented with different frequencies and intensities of tones and shocks on two consecutive days. **(B)** Frequency tuning in LA somata. From left to right, frequency tuning of three example neurons and population average (mean ± SEM, n = 94 neurons from 7 mice). **(C)** Tone intensity tuning in LA somata. From left to right, frequency tuning of three example neurons and population average (mean ± SEM, n = 94 neurons from 7 mice). **(D)** Shock intensity tuning in LA somata. From left to right, frequency tuning of three example neurons and population average (mean ± SEM). The population response increases with shock intensity (One-way ANOVA $F(4,465) = 5.162$, $p < 0.001$, n = 94 neurons from 7 mice). **(E)** Similar frequency tuning in the somata and dendrites of a LA PNs. From left to right, frequency tuning in the soma and three dendrites of an example LA PN (mean ± SEM). **(F)** Similar tone intensity in the somata and dendrites of a LA PNs. From left to right, frequency tuning in the soma and three dendrites of an example LA PN (mean ± SEM). **(G)** Similar shock intensity tuning in the somata and dendrites of a LA PNs. From left to right, frequency tuning in the soma and three dendrites of an example LA PN (mean ± SEM).

## CS tones induce isolated dendritic activity in naïve animals

We next characterized the features of soma-dendrite coupling during tone presentations in naïve animals. In contrast to spontaneous events, the amplitude of tone-locked dendritic $Ca^{2+}$ transients was larger in dendrites than in their parent somata (Fig. 17A), suggesting that tone presentations induce a stronger activity in dendrites. Consistent with this observation, the proportion of dendrite-specific $Ca^{2+}$ transients was larger during tone presentations than during spontaneous activity (Fig. 17B). Furthermore, the amplitude of dendrite-specific $Ca^{2+}$ transients was larger during tones than during spontaneous activity (Fig. 17C). To eliminate possible confounds caused by the animal's motion, we compared the relative somatic and dendritic event amplitude during rest and locomotion. The frequency of somatic $Ca^{2+}$ transients was elevated during locomotion (Fig. 19B) but the relative amplitude of $Ca^{2+}$ transients detected in dendrites and somata was similar (Fig. S19C), indicating that locomotion has little effect on soma-dendrite coupling. Taken together, these results show that dendritic activity in LA PNs is enhanced during tone presentations in naïve animals.

### Somatostatin interneurons control dendrite-specific activity

Much like in the neocortex, the BLA is organized in neuronal microcircuits involving local inhibitory interneurons that tightly control PNs activity. SST interneurons form GABAergic synapses onto PN dendrites and are inhibited during tone presentations (*24*, *25*), suggesting a role in gating dendritic excitability of LA PNs (*64*).

We tested this hypothesis by suppressing SST interneurons activity pharmacologically by expressing an engineered receptor exclusively activated by the ligand Clozapine N-oxide (CNO). In the presence of CNO, hM4D(Gi) activation results in hyperpolarization and inhibition of neuronal activity (*65*). We imaged somatic and dendritic activity of LA PNs in the presence of CNO versus saline control during tone presentation (Fig. 20A-C).

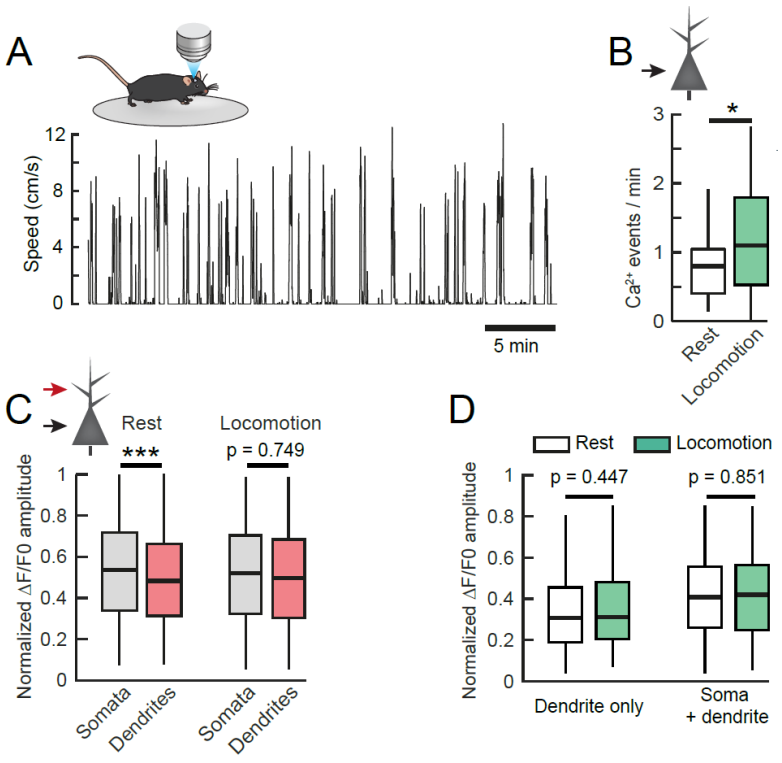


**Fig. 19. Locomotion does not affect the proportion of dendrite-specific transients.**

**(A)** Example running speed recording from a head-restrained mouse. **(B)** Somatic $Ca^{2+}$ transients are more frequent during locomotion than during rest (p = 0.013, Student's T-test, n = 94 neurons). Box-and-whisker plots show median values and 25th and 75th percentiles, the maximum whiskers length is 1.5 times the interquartile range. **(C)** Left: $Ca^{2+}$ transients during rest have a larger normalized amplitude in somata than in dendrites. Right: $Ca^{2+}$ transients during locomotion have similar normalized amplitude in somata and in dendrites (rest, p < 0.001, locomotion, p = 0.749, both Wilcoxon signed-rank test, n = 5390 transients during rest, n = 1933 transients during locomotion from 189 soma-dendrite pairs). **(D)** Similar proportion of dendrite-specific transients during rest and locomotion periods (Fisher's exact test, n = 5390 transients during rest, n = 1933 transients during locomotion from 189 soma-dendrite pairs).

In saline controls, a larger proportion of dendrite-specific $Ca^{2+}$ events occurred during tones as compared to during spontaneous activity (Fig. 20D-E), while the amplitude of dendrite-specific $Ca^{2+}$ transients was larger during tones (Fig. 20F), as shown in naïve mice. In contrast, suppression of SST interneuron activity upon delivery of CNO abolished this effect and led to a decrease in the proportion and the amplitude of shared somatic and dendritic events during tones (Fig. 20G-I). In addition, suppressing SST interneuron activity increased the proportion of dendrite-specific $Ca^{2+}$ transients during spontaneous activity, but not

during tones (Fig. 20J). Reduced SST interneuron activity also led to decreased functional correlation between dendrites and their parent somata (Fig. 20K). Furthermore, the distance dependence of the soma-dendrite response correlation (Fig. 20L) was abolished and the amplitude of somatic and dendritic $Ca^{2+}$ events was less correlated (Fig. 20M), suggesting that upon SST disinhibition, dendritic activity is able to propagate more efficiently to the soma.

Taken together, these results show that SST interneurons reduce spontaneous, but not tone-locked dendritic activity in LA PNs. We propose that under physiological conditions, SST interneuron suppression disinhibits LA PNs dendrites during tones, leading to increased local dendritic activity. By suppressing SST interneurons, we unmask their gating effect on spontaneous dendritic activity. In this framework, dendritic integration of sensory input is actively regulated by a local inhibitory microcircuit, but it is unknown how it is affected by learning.

## Fear conditioning induces specific changes in LA principal neurons somatic CS responses

Fear conditioning induces a reorganization of somatic CS responses in BLA PNs (*51*, *66*) and the plasticity most likely occurs at the synaptic level in dendrites (*67*, *68*). However, it remains unknow how these changes in dendritic responses develop during fear learning.

In order to interpret changes in sensory stimulus representation during learning, we first focused our analysis on the baseline stability of somatic responses and the overlap between tone and shock-responsive neurons in naïve animals (Fig. 21A-C). The probability of tone response in a single neuron on two consecutive days was highly correlated (Fig. 21D) while the probability of tone and shock response was less correlated (Fig. 21E). In fact, the neuronal response identity (excited, inhibited, or unresponsive) of most neurons was preserved over days (Fig. 22A).

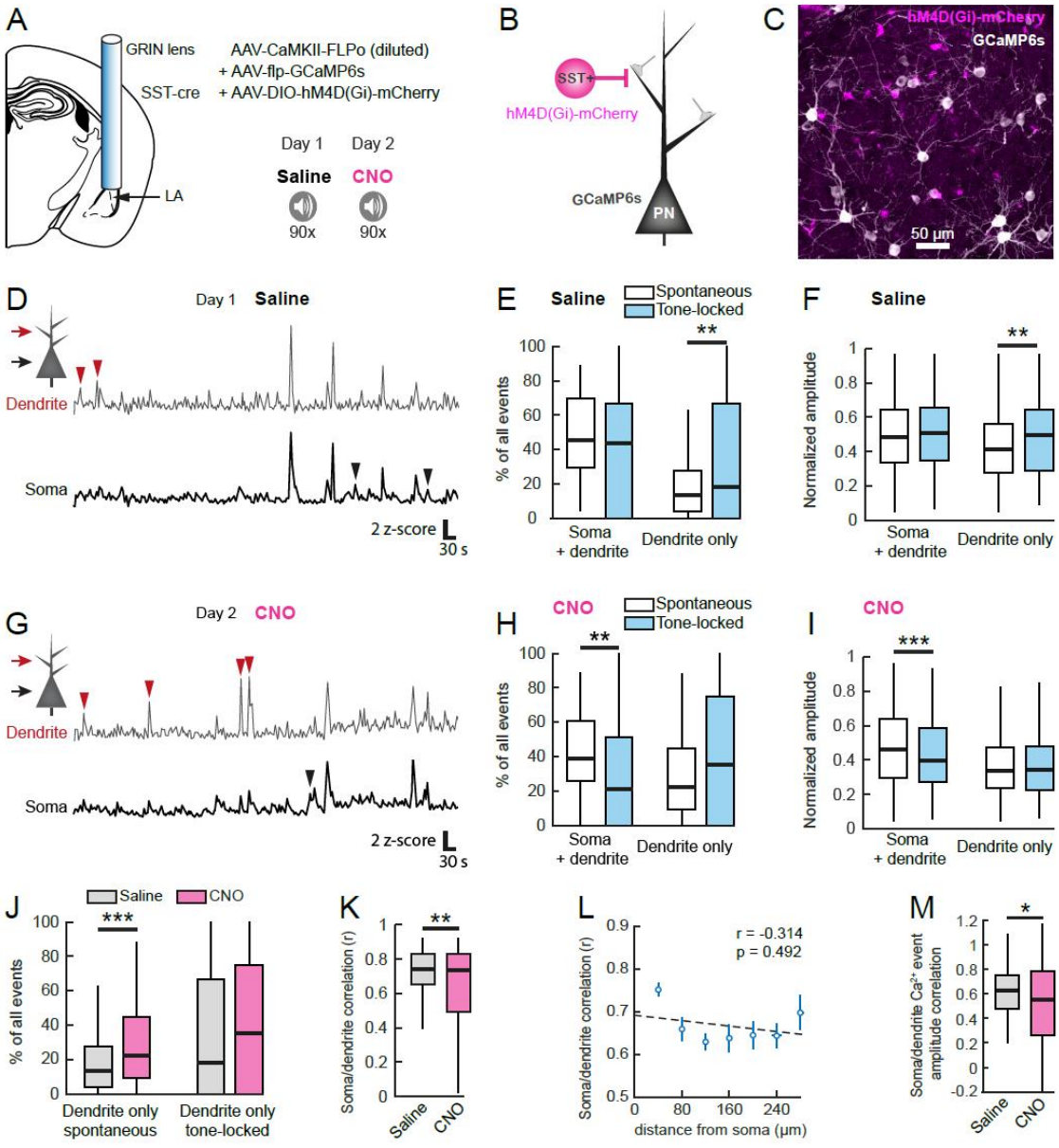


**Fig. 20. Suppression of SST interneuron activity increases spontaneous dendritic activity.**

**(A)** Combination of Cre and Flp-dependent viral constructs to express hM4D(Gi) in SST interneurons and GCaMP6s in a sparse population of LA PNs. Animals were presented with 90 tones after saline or intraperitoneal CNO injection on two consecutive days. **(B)** Experimental scheme. **(C)** Confocal image of HM4D(Gi)-mCherry in SST interneurons and sparse GCaMP6s in LA PNs. **(D)** Little dendrite-specific $Ca^{2+}$ activity after saline control injection in an example soma-dendrite pair. Arrowheads indicate compartment-specific $Ca^{2+}$ transients. **(E)** Higher proportion of dendrite-specific $Ca^{2+}$ transients during tone than during spontaneous activity after saline control injection (dendrite only, p = 0.006, soma + dendrite, p = 0.078, all Wilcoxon signed-rank test, n = 7036 spontaneous and 843 tone-locked transients from 142 soma-dendrite pairs). **(F)** Higher amplitude of dendrite-specific $Ca^{2+}$ transients during tone than during spontaneous activity

after saline control injection (dendrite only, p = 0.003, soma + dendrite, p = 0.125, both Mann-Whitney U-test, n = 7036 spontaneous and 843 tone-locked transients from 142 soma-dendrite pairs). **(G)** Suppression of SST interneuron activity by CNO injection increases dendrite-specific $Ca^{2+}$ activity. Arrowheads indicate compartment-specific $Ca^{2+}$ transients in an example soma-dendrite pair. **(H)** Lower proportion of shared somatic and dendritic transients, but similar proportion of dendrite-specific transients during and outside tone upon suppression of SST interneuron activity (dendrite only, p = 0.135, soma + dendrite, p = 0.006, both Wilcoxon signed-rank test, n = 6644 spontaneous and 660 tone-locked transients from 142 soma-dendrite pairs). **(I)** Lower amplitude of shared somatic and dendritic transients, but similar proportion of dendrite-specific transients during and outside tone upon suppression of SST interneuron activity (dendrite only, p = 0.709, soma + dendrite, p < 0.001, both Mann-Whitney U-test, n = 6644 spontaneous and 660 tone-locked transients from 142 soma-dendrite pairs). **(J)** Suppression of SST interneuron activity increases spontaneous, but not tone locked dendrite-specific activity in LA PNs (spontaneous, p < 0.001 , tone locked, p = 0.222, both Wilcoxon signed-rank test, 142 soma-dendrite pairs). **(K)** Suppression of SST interneuron activity decreases soma-dendrite coupling. Pearson's correlation between somatic and dendritic $Ca^{2+}$ activity traces (p < 0.007, Student's T-test, n = 79 dendritic segments from 14 neurons). **(L)** Suppression of SST interneuron activity abolishes distance dependency of soma-dendrite correlation (Pearson's correlation between somatic and dendritic $Ca^{2+}$ activity traces, n = 79 dendritic segments from 14 neurons). **(M)** Suppression of SST interneuron activity decreases the slope of soma-dendrite activity correlation (p = 0.031, Wilcoxon signed-rank test, n = 79 dendritic segments from 14 neurons). Box-and-whisker plots show median values and $25^{th}$ and $75^{th}$ percentiles, the maximum whiskers length is 1.5 times the interquartile range.

In order to probe CS response plasticity in dendrites and somata of LA PNs, we then performed a 3-day differential auditory fear conditioning paradigm in a different group of mice while recording dendritic as well as somatic $Ca^{2+}$ activity in head fixed mice under a two-photon microscope (Fig. 23A). The fear behavior (freezing) was tested in freely moving conditions and mice learned the CS-US association as indicated by higher freezing levels to the CS+ after conditioning (Fig. 23B).

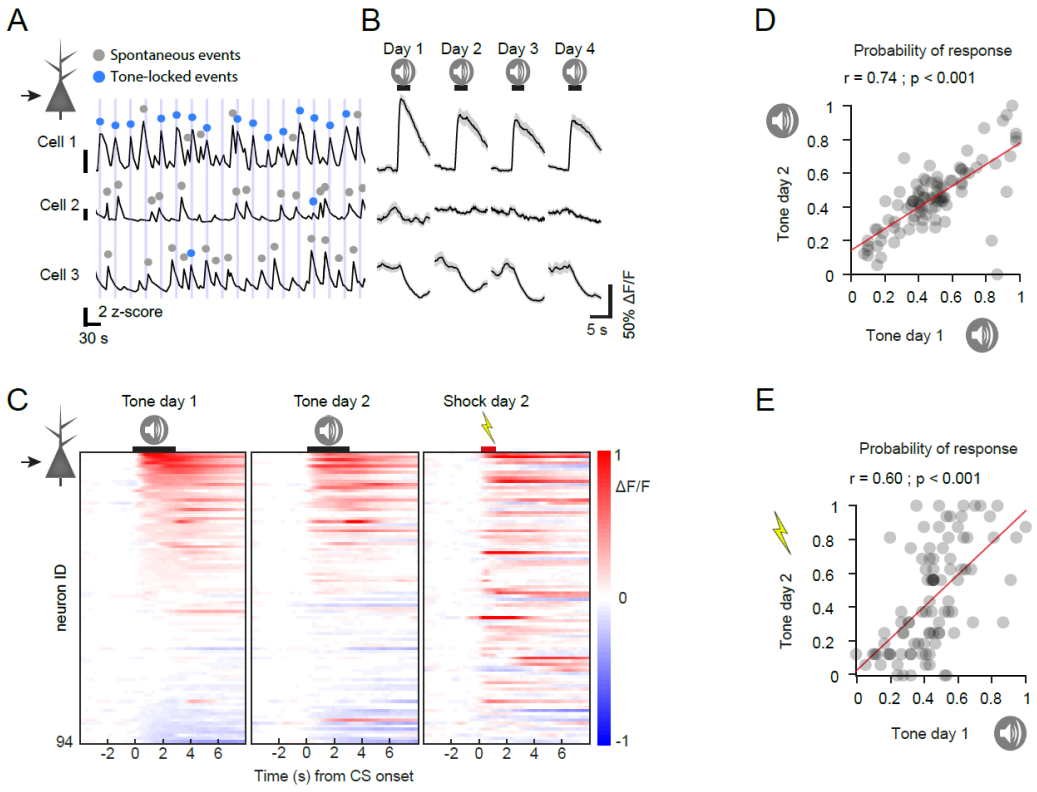


**Fig. 21. Overlap and stability of tone and shock somatic responses in naïve animals.**

**(A)** $Ca^{2+}$ activity of three neurons with different tone responses. Blue vertical lines represent the tone periods, gray dots represent transients detected outside of the tone, blue dots represent transients detected during the tone. **(B)** Tone response dynamics are preserved over days. Average tone responses from neurons in (A), from a subset of mice presented with tones over 4 consecutive days. **(C)** Tone responses are stable over days in naïve animals. Data are averaged over all trials and ordered according to their tone response amplitude on day 1. The population of neurons active on day 1 and day 2 are similar and have little overlap with the shock-responsive population. **(D)** Probabilities of tone response on day 1 and 2 are highly correlated ($r = 0.74$, $p < 0.001$). **(E)** Probabilities of tone and shock responses are correlated ($r = 0.60$, $p < 0.001$).

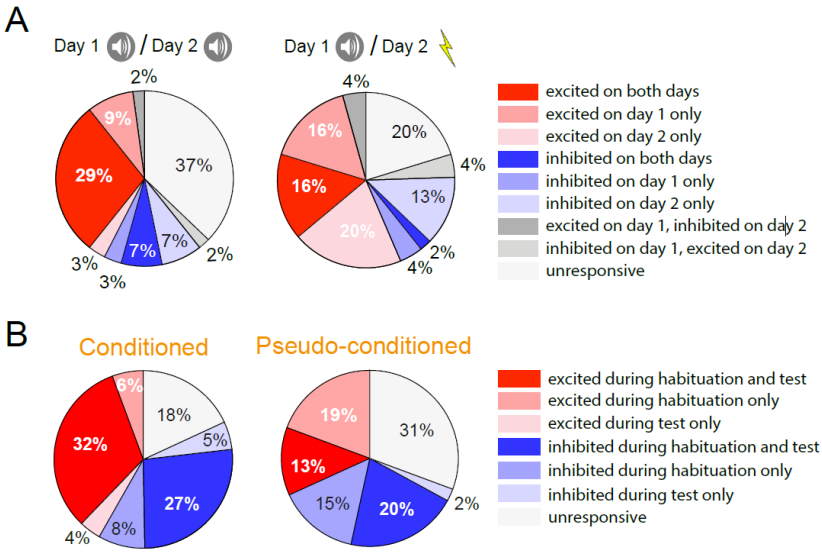


**Fig. 22. Proportions of responsive neurons over days.**

**(A)** Neuronal response comparing proportions of responsive neurons on day 1 and 2 of tone and shock presentations (see Fig. 8a). Left, comparing proportions of tone responsive neurons on day 1 and 2. Most neurons responsive on one day 1 are also responsive on day 2. Right, proportions of tone responsive neurons on day 1 and shock-responsive neurons on day 2 (C-F: n = 94 somata from N = 7 mice. **(B)** Proportions of tone responsive neurons before and after fear conditioning (left, n = 177 somata from N = 9 mice) or pseudo-conditioning (right, n = 88 somata from N = 6 mice).

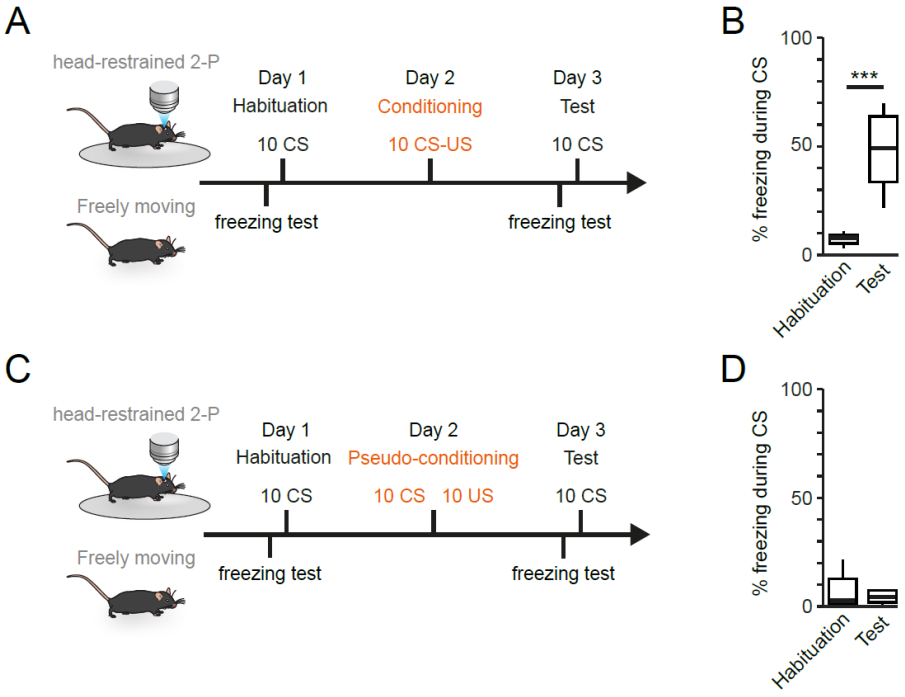

**Fig. 23. Head-retrained fear conditioning and pseudo-conditioning paradigms.**

**(A)** Auditory fear conditioning paradigm with simultaneous two-photon imaging. Freezing tests were performed in freely moving conditions. **(B)** Mice learn the CS-US association. Percent time spent freezing, during the CS before and after learning (habituation day: 8.4 ± 1.6%, test day: 47.8 ± 5.6%, N = 9 mice, $p < 0.001$, Wilcoxon signed-rank test). Error bars indicate SEM. **(J)** Pseudo- (unpaired) fear conditioning paradigm with simultaneous two-photon imaging. Freezing tests were performed in freely moving conditions. **(K)** Percent time spent freezing during the CS, before and after learning (habituation: 6.83 ± 3.43 %, test: 6.84 ± 3.42 %, N = 6 mice, $p = 0.7814$, Wilcoxon signed-rank test). Error bars indicate SEM.

Upon fear conditioning, a large fraction of somata (58.8% of 177 recorded PNs from N = 9 mice) preserved their CS response identity (excited or inhibited by the tone), while 23.1% of all recorded neurons (n = 41) exhibited plastic CS responses. The remaining 18.1% LA PNs (n = 32) were not CS responsive (Fig. 22B). At the population level, the mean CS response amplitude over all somata after fear conditioning was stable (Fig. 24A-C). Somatic plasticity of CS responses was bidirectional, with a population of neurons significantly increasing their CS response during learning (CS upregulated, CSup) and another population significantly decreasing their CS response (CS downregulated, CSdown) (Fig. 25A-B) as previously observed in another study (*51*).

We next tested whether the dynamics of CS responses were driven by changes in CS response amplitude or CS response probability. Our results show that both the probability and the amplitude of CS responses are higher in CSup neurons than in CSdown neurons (Fig. 25 C-D). Therefore, bidirectional plasticity in both the probability and amplitude of CS responses occur during learning and contribute to the emergence of CSup and CSdown LA PN populations.

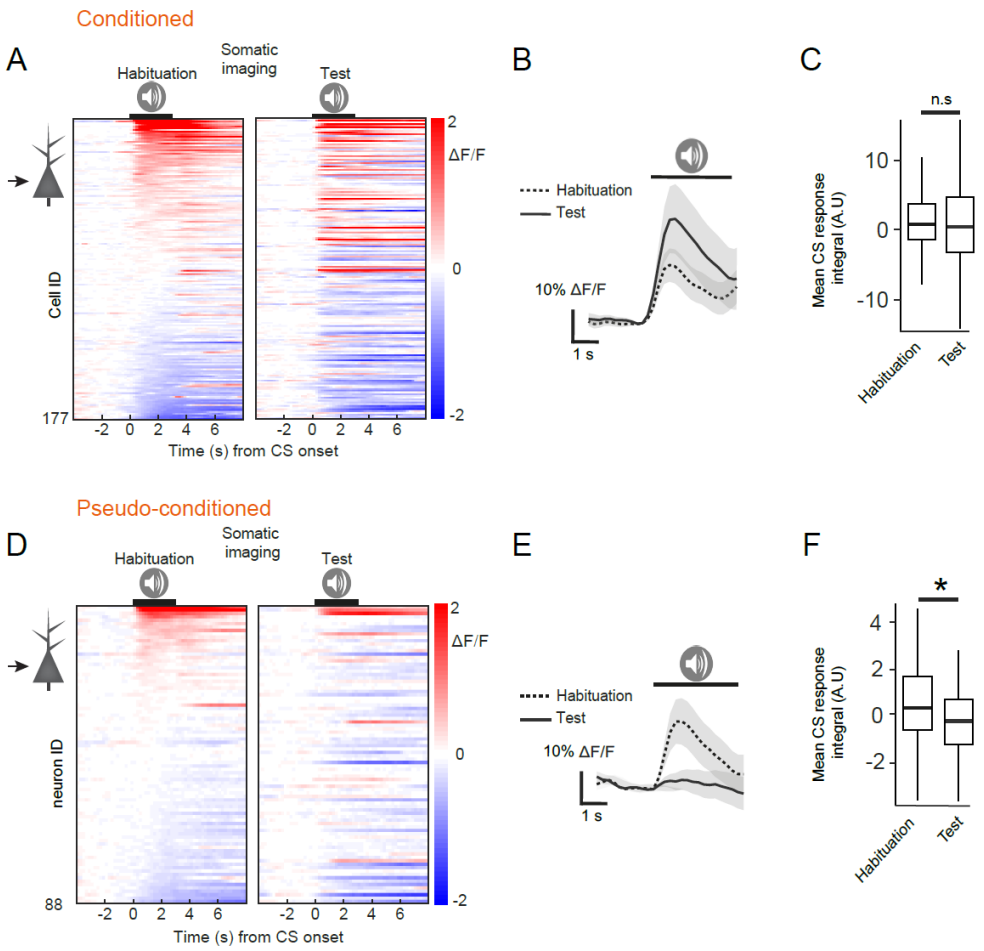


## Fig. 24. Stable CS response in LA somata upon fear conditioning.

**(A)** CS responses in somata during fear learning. Data are averaged over 10 trials and ordered according to CS response amplitude during habituation (n = 177 somata). **(B)** Mean tone responses of all somata before and after fear conditioning (n = 177, mean ± SEM). **(C)** The mean somatic CS response is similar before and after learning (p = 0.270, Wilcoxon signed-rank test). **(D)** CS responses in somata during pseudo-conditioning. Data are averaged over 10 trials and ordered according to CS response amplitude during habituation (n = 88 somata). **(E)** Mean tone responses of all somata before and after pseudo-conditioning (n = 88, mean ± SEM). **(F)** Decreased mean somatic CS response after pseudo-conditioning (p = 0.0125, Wilcoxon signed-rank test). Box-and-whisker plots show median values and 25$^{th}$ and 75$^{th}$ percentiles, the maximum whiskers length is 1.5 times the interquartile range.

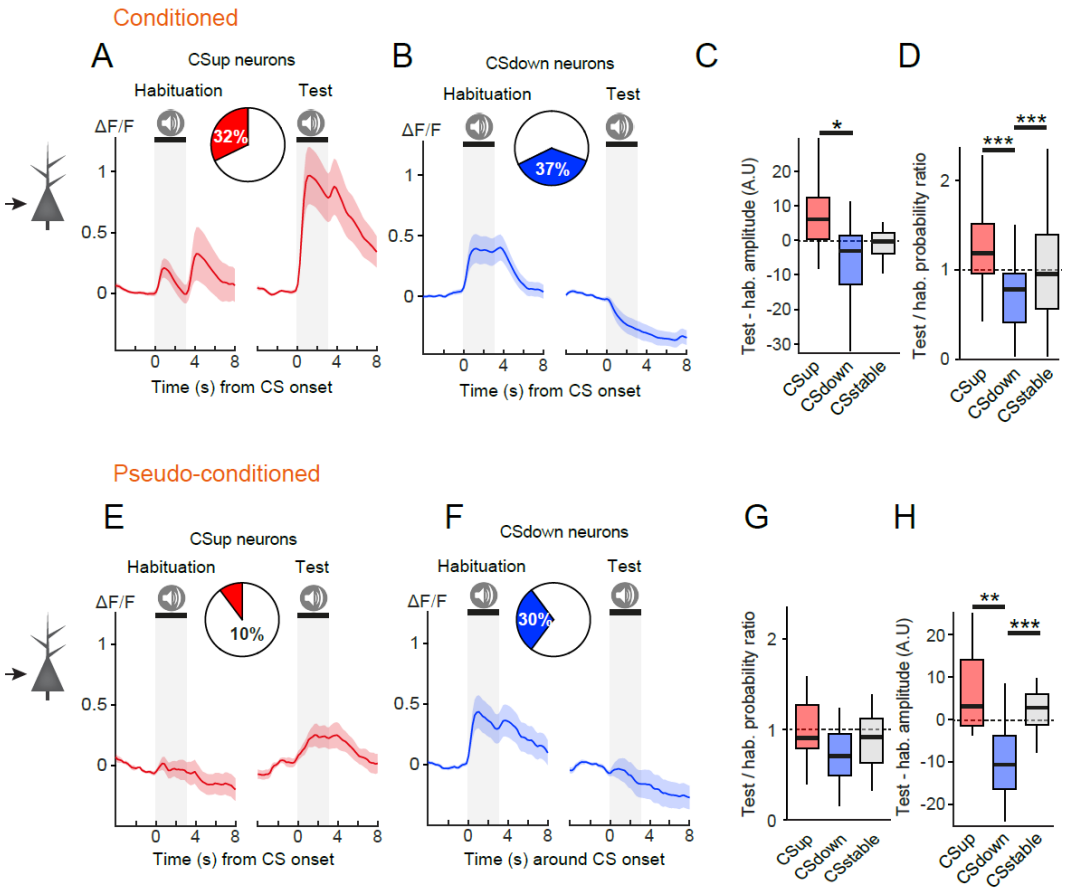


**Fig. 25. CS response dynamics in LA somata during auditory fear conditioning and pseudo-conditioning.**

**(A-B)** A large proportion of neurons upregulate (A) and downregulate (B) their CS response during learning (mean ± SEM). **(C)** CS response probability ratio per cell before and after conditioning. After conditioning, the CS response probability ratio is higher in CSup neurons than in CS-downregulated neurons ($p < 0.001$) and lower in CS-downregulated neurons than in CS stable neurons ($p < 0.001$, One-way ANOVA $F(2,138) = 21.019$, $p < 0.001$, Bonferroni correction for multiple comparison). Data are normalized to the habituation day. **(D)** CS response amplitude ratio per cell before and after fear conditioning. After fear conditioning, the CS response amplitude ratio similar across the functional cell types (One-way ANOVA $F(2,124)=0.765$, $p=0.468$, Bonferroni correction for multiple comparison). Data are normalized to the habituation day. **(E-F)** A small proportion of neurons upregulate (E) and a large proportion downregulate (E) their CS responses during learning (n = 9 CSup, n = 26 CSdown neurons from N = 6 mice, mean ± SEM). **(G)** CS response probability ratio per cell before and after pseudo-conditioning. After conditioning, CS response probability ratio is higher in CSup neurons than in CS-downregulated neurons ($p = 0.0246$, One-way ANOVA $F(2,47) = 4.136$, $p = 0.022$, Bonferroni correction for multiple comparison). Data are normalized to the habituation day. **(H)** CS response amplitude ratio per cell before and after pseudo-conditioning. After fear conditioning, the CS response amplitude ratio is higher in CSup

neurons than in CS-downregulated neurons (p = 0.0112, One-way ANOVA F(2,46) = 5.752, p = 0.006, Bonferroni correction for multiple comparison). Data are normalized to the habituation day. Box-and-whisker plots show median values and 25$^{th}$ and 75$^{th}$ percentiles, the maximum whiskers length is 1.5 times the interquartile range.

In a classical Hebbian learning framework, the US acts as a teaching signal that instructs neurons to undergo potentiation of the CS response (*69*), giving rise to the prediction that only US-responsive cells upregulate their CS response. However, we found that a similar proportion of CSup and CSdown neurons were US-responsive (Fig. 26F-G), p = 0.527, Fisher's exact test. These results indicate that US responsiveness does not determine the direction of CS response plasticity in single neurons.

In order to disentangle the specific contribution of the CS-US association from baseline somatic plasticity of CS responses over days, we performed pseudo- (unpaired) fear conditioning in a separate cohort of mice, where the CS and the US were presented independently (more than 120 seconds apart) on the conditioning day (Fig. 23C). As expected, pseudo-conditioned mice did not freeze to the CS (Fig. 23D), indicating that they did not form a CS-US associative memory. During pseudo-conditioning, 21.6% of the recorded somata lost their CS responsiveness (n = 19 of 88 recorded neurons; 19.3% excitatory, 2.3% inhibitory) and only 15% acquired a CS response, all inhibitory (Fig. 22B, n = 13; 0% excitatory, 15% inhibitory). On the test day, and in contrast to fear conditioning, pseudo-conditioning resulted in a reduction of somatic CS response amplitudes at the population level (Fig. 24D-F).

Furthermore, CSup neurons were overrepresented in conditioned mice compared to pseudo-conditioned mice, while CSdown neurons were found in similar proportions in both groups (Fig. 25E-F and Fig. 26C). Thus, fear conditioning induces plasticity in a specific neuronal population that increases CS responses beyond changes attributable to adaptation, general drift or passage of time.

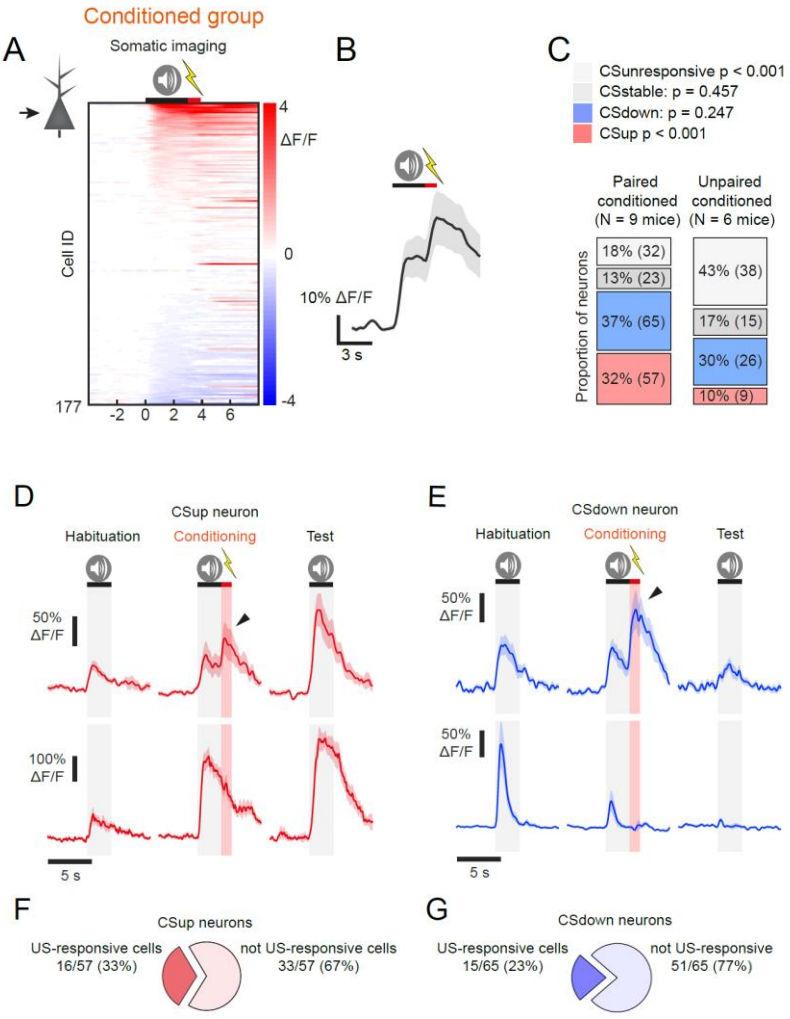


**Fig. 26. Somatic activity during CS-US pairing and proportions of functionally defined cell types.**

**(A)** CS responses in somata on the second day of fear conditioning (see Fig. 4). Data are averaged over 10 trials and ordered according to CS response amplitude (n = 177 somata from 9 mice). **(B)** Mean response of all somata during CS-US pairings (n = 177, mean ± SEM). **(C)** A larger proportion of neurons upregulate their CS response during fear conditioning than during pseudo-conditioning. More neurons remain unresponsive to the CS in the pseudo-conditioned group. The numbers of neurons in each category is indicated within brackets (Fisher's exact test, n = 177 neurons from 9 fear conditioned mice, n = 88 neurons from 6 pseudo-conditioned mice). **(D)** CS response of an example CSup, US-responsive neuron (top) and of a CSup, not US-responsive neurons (bottom) during fear conditioning (mean ± SEM over 10 CS-US pairings). The black arrowhead indicates the US response. **(E)** CS response of an example CSdown, US-responsive neuron (top) and of a CSdown, not US-responsive neurons (bottom) during fear conditioning. **(F)** Proportion of US-responsive and not US-responsive neurons among CSup neurons (n = 57 CSup neurons). **(G)** Proportion of US-responsive and not US-responsive neurons among CSdown neurons (n = 65 CSdown neurons).

## Associative fear conditioning induces CS response potentiation in LA PN dendrites

Given that tones increase the amount of localized dendritic activity in LA PNs (Fig. 17B-C), which is controlled by local inhibitory interneurons (Fig. 20H-I), we reasoned that fear conditioning could induce a compartment-specific CS response plasticity in LA PN dendrites and somata. Indeed, in contrast to somata, the mean CS response in dendrites exhibited a net increase after fear conditioning (Fig. 27A-C), driven by a large fraction of CSup dendrites compared to a small fraction of CSdown dendrites (Fig. 28A-B). We also observed similar dynamics in individual dendritic spines of LA PNs (Fig. 29A), again in contrast to somatic dynamics (Fig. 27A-C).

Interestingly, the mean tone response of LA PN dendrites of pseudo-conditioned mice underwent a net decrease (Fig. 27D-F), similar to the soma (Fig. 24D-F). Accordingly, a large proportion of dendrites were CSdown (Fig. 28E-F), indicating that the net CS response increase observed in the dendrites of conditioned mice's requires the pairing of the CS with the US. Together, these results show that while learning induces bidirectional somatic plasticity of CS responses, it leads predominantly to CS response upregulation in dendrites and in spines, raising the question of how CS response plasticity occurs in different subcellular compartments in single neurons.

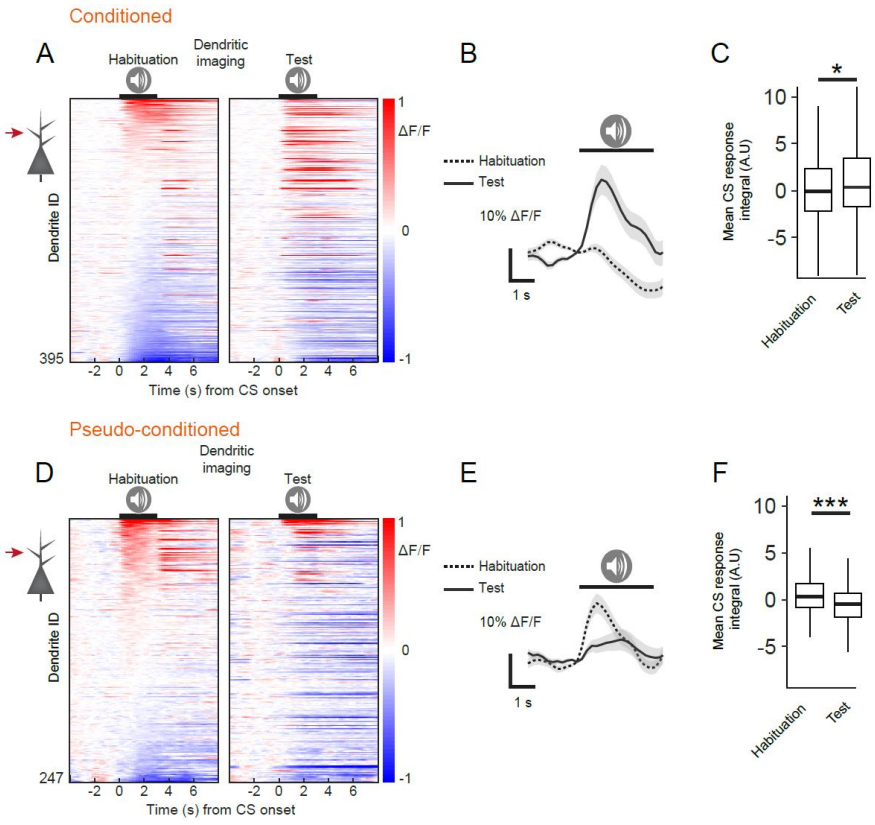


**Fig. 27. Increased CS response in LA PNs dendrites upon fear conditioning.**

**(A)** CS responses in dendrites during fear conditioning. Data are averaged over 10 trials and ordered according to CS response amplitude during habituation (n = 395 dendrites from 9 mice). **(B)** Mean tone response of all dendrites before and after fear conditioning (n = 395, mean ± SEM). **(C)** The mean CS response increases in dendrites during learning ($p = 0.035$, Wilcoxon signed-rank test). **(D)** CS responses in dendrites during pseudo-conditioning. Data are averaged over 10 trials and ordered according to CS response amplitude during habituation (n = 247 dendrites from 6 mice). **(E)** Mean tone response of all dendrites before and after fear conditioning (n = 247, mean ± SEM). **(F)** The mean CS response decreases in dendrites during pseudo-conditioning ($p < 0.001$, Wilcoxon signed-rank test). Box-and-whisker plots show median values and 25$^{th}$ and 75$^{th}$ percentiles, the maximum whiskers length is 1.5 times the interquartile range.

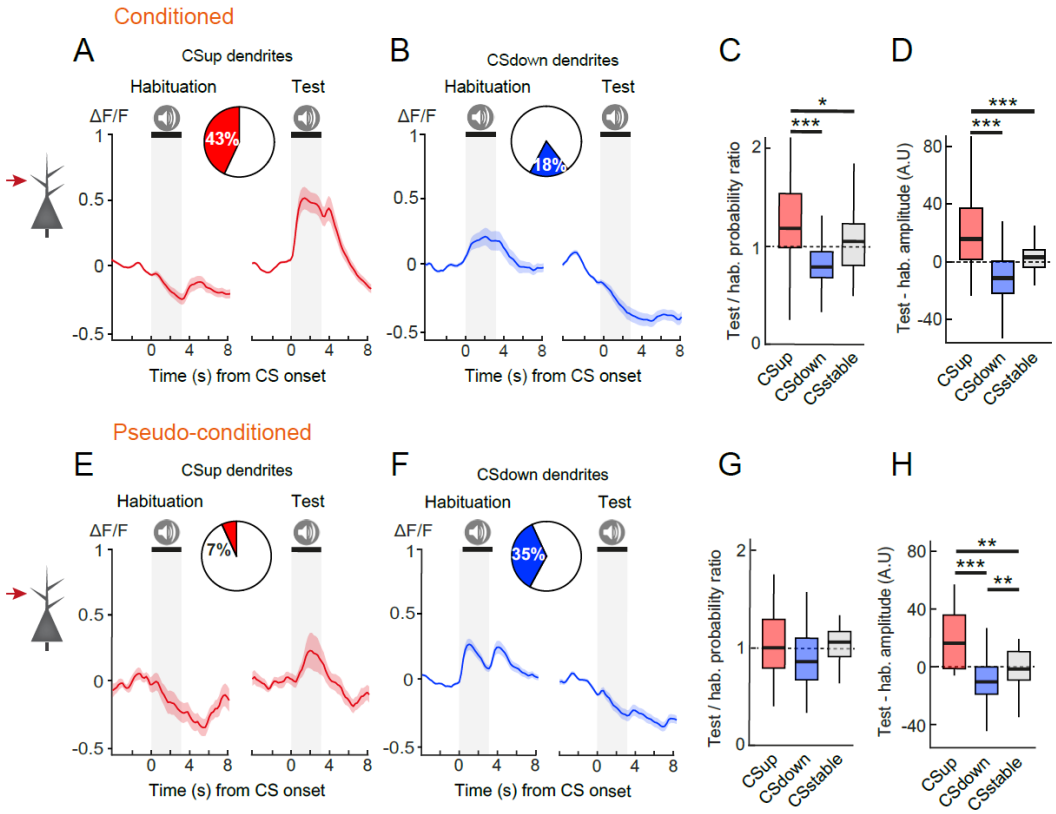


**Fig. 28. CS response dynamics in LA PNs dendrites during auditory fear conditioning and pseudo-conditioning.**

**(A-B)** A large proportion of dendrites up-regulate (A) and a smaller proportion down-regulate (B) their CS response during learning (mean ± SEM). **(C)** CS response probability ratio per dendrite before and after learning (One-way ANOVA $F(2,127) = 2.651$, $p = 0.075$, Bonferroni correction for multiple comparison). Data are normalized to the habituation day. **(D)** CS response amplitude ratio per dendrite before and after learning. (One-way ANOVA $F(2,127) = 23.424$, $p < 0.001$, Bonferroni correction for multiple comparison). Data are normalized to the habituation day. **(E-F)** A small proportion of dendrites up-regulate (E) and a large proportion down-regulate (F) their CS response during pseudo-conditioning (mean ± SEM). **(G)** CS response probability ratio per dendrite before and after pseudo-conditioning (One-way ANOVA $F(2,127) = 2.651$, $p = 0.075$, Bonferroni correction for multiple comparison). Data are normalized to the habituation day. **(H)** CS response amplitude ratio per dendrite before and after pseudo-conditioning (One-way ANOVA $F(2,127) = 23.424$, $p < 0.001$, Bonferroni correction for multiple comparison). Data are normalized to the habituation day. Box-and-whisker plots show median values and 25$^{th}$ and 75$^{th}$ percentiles, the maximum whiskers length is 1.5 times the interquartile range.

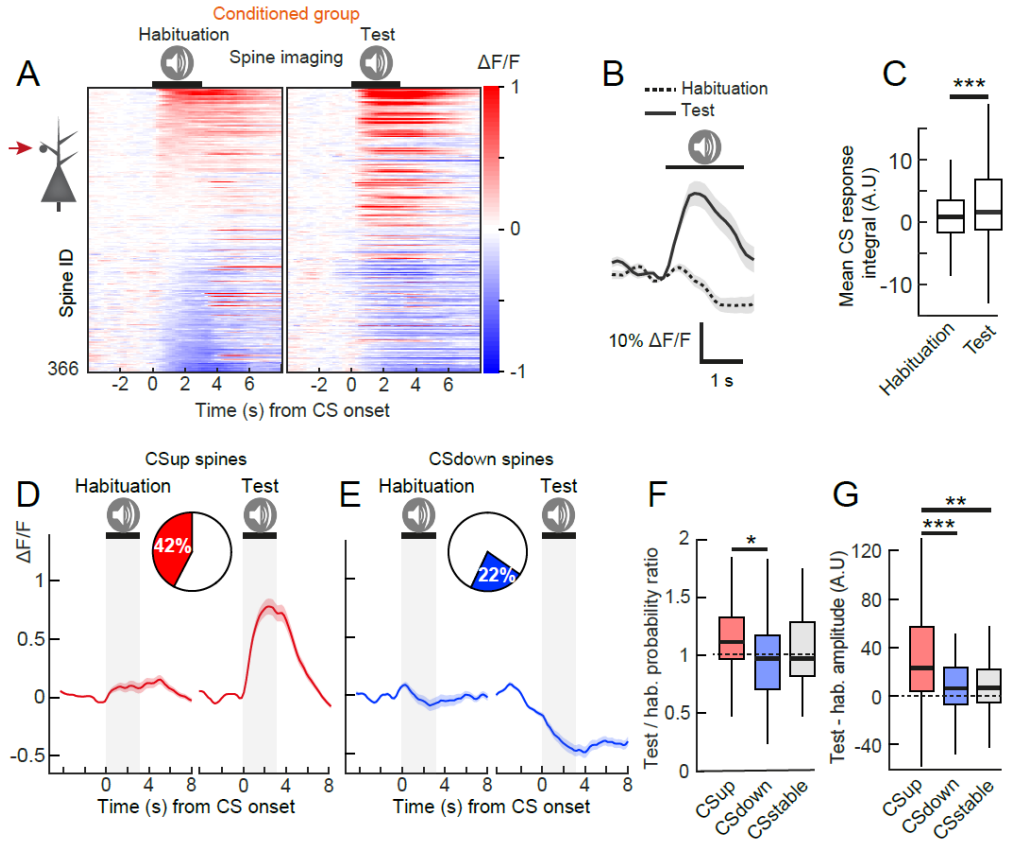


**Fig. 29. CS response dynamics in LA PNs spines during auditory fear conditioning.**

**(A)** CS responses in dendritic spines during fear conditioning. Data are averaged over 10 trials and ordered according to CS response amplitude during habituation (n = 366 dendritic spines from 9 mice). **(B)** Mean tone response of all spines before and after fear conditioning (n = 366, mean ± SEM). **(C)** The mean CS response increases in dendritic spines during learning ($p < 0.001$, Wilcoxon signed-rank test). **(D-E)** A large proportion of dendritic spines up-regulate (D) and a smaller proportion down-regulate (E) their CS response during learning (mean ± SEM). **(F)** CS response probability ratio per dendritic spine before and after learning (One-way ANOVA $F(2,47) = 4.136$, $p = 0.022$, Bonferroni correction for multiple comparison). Data are normalized to the habituation day. **(G)** CS response amplitude ratio per dendritic spine before and after learning. (One-way ANOVA $F(2,46) = 5.752$, $p = 0.006$, Bonferroni correction for multiple comparison). Data are normalized to the habituation day. Box-and-whisker plots show median values and 25$^{th}$ and 75$^{th}$ percentiles, the maximum whiskers length is 1.5 times the interquartile range.

## Somatic and dendritic CS response plasticity is uncoupled in CSdown neurons

Given the variability in the correlation of soma-dendrite $Ca^{2+}$ activity in single neurons (Fig. 16D) and following the observation that CS responses undergo a net increase in LA PN

dendrites but not in somata during learning (Fig. 24A-C and Fig. 27A-C), we hypothesized that fear learning leads to further decorrelation between the dendritic branches of single neurons.

Indeed, we found that the extent of CS response plasticity was variable between the different dendrites of single neurons (Fig. 30A). In addition, the variability of CS response amplitude increased after fear conditioning while the variability of CS response probability remained stable (Fig. 30B-C). Furthermore, somatic and dendritic activity became more decorrelated after fear conditioning (Fig. 30D), indicating that plasticity of CS responses can be specific to individual dendritic branches, leading to a more decorrelated activity between soma and dendrites. Importantly, these effects were not observed in pseudo-conditioned mice, indicating that they are specifically induced by associative learning. Such a decorrelation of somatic and dendritic activity during learning raises the question of how dendritic plasticity of CS response relates to somatic plasticity in single neurons. We therefore asked whether different plasticity dynamics in dendrites could underlie the somatic plasticity characterizing CSup and CSdown neurons.

To this end, we compared somatic and dendritic plasticity of CS responses in CSup and CSdown neurons (Fig. 31A,D). We found that in CSup neurons, in addition to the soma, the probability and the amplitude of dendritic CS responses also increased (Fig. 31B-C), indicating that somatic plasticity reflects dendritic plasticity in these neurons. In contrast, the probability of CS responses decreased in CSdown neurons somata but remained stable in their dendrites (Fig. 31E-F). Such uncoupled somatic and dendritic plasticity of CS response indicates that the somatic output of LA PNs does not automatically reflect the plasticity of CS response occurring in the dendrites.

Overall, these results show that over the course of learning, CS responses develop differently between dendrites of single LA PNs, in some cases independently from the soma. Our data also suggest that somatic plasticity of CS response during learning only partially reflects dendritic plasticity and that somatic output could be further regulated.

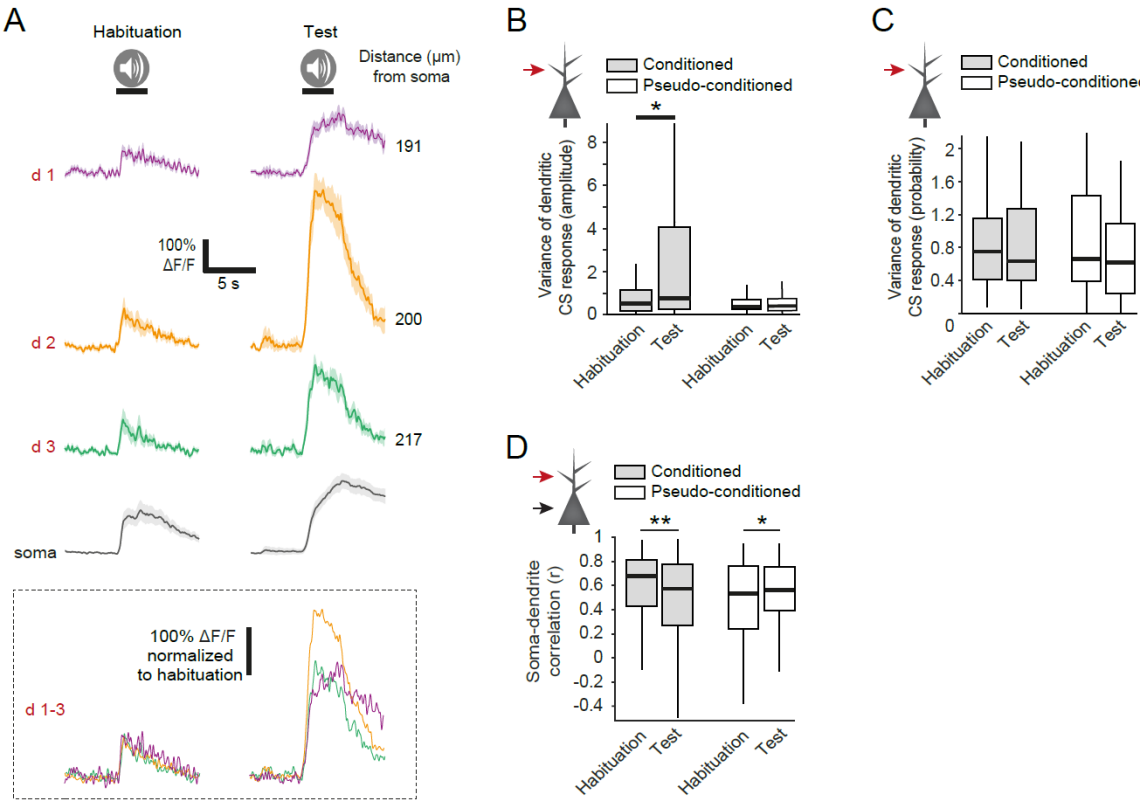


**Fig. 30. Variability of dendritic CS response during fear conditioning.**

**(A)** Variability of CS responses between three dendritic segments and the soma of the same neurons during conditioning (mean ± SEM). The bottom panel show the mean CS response in the three dendrites normalized to the habituation day. **(B)** The variance of CS response amplitude increases between dendrites during fear conditioning (p = 0.010, both Student's t-test, n = 250 dendrites from 50 somata from N = 9 mice). **(C)** The variance of dendritic CS response probability between dendrites remains similar during fear conditioning (p = 0.974, Student's t-test, n = 250 dendrites from 50 somata from N = 9 mice). **(D)** Soma-dendrite coupling decreases during fear conditioning (Pearson's correlation between somatic and dendritic $Ca^{2+}$ traces, p = 0.003, Wilcoxon signed-rank test, n = 235 dendritic segments). Box-and-whisker plots show median values and 25$^{th}$ and 75$^{th}$ percentiles, the maximum whiskers length is 1.5 times the interquartile range.

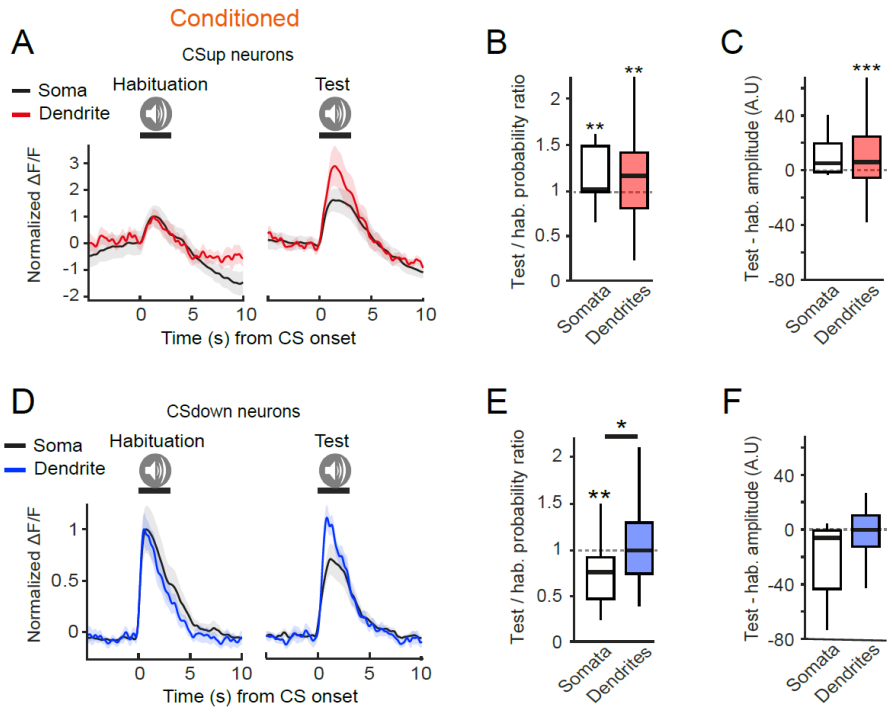


**Fig. 31. Uncoupling of somatic and dendritic plasticity of CS response during fear learning.**

**(A)** CS response of an example CSup soma and dendrite of the same neuron before (habituation) and after (test) fear conditioning. Upon learning, CS response increases in both the soma and dendrite. Data are normalized to the habituation day (mean ± SEM). **(B)** CS response of an example CSdown soma and dendrite of the same neuron before (habituation) and after (test) fear conditioning. Upon learning, the CS response decreases in the soma but not in the dendrite. Data are normalized to the habituation day (mean ± SEM). **(C)** CS response probability test over habituation ratio in somata and dendrites. During fear conditioning, the CS response probability of CSup neurons increases in somata ($p = 0.003$, Wilcoxon signed-rank test) and in dendrites ($p = 0.002$, Wilcoxon signed-rank test). CS response probability increases similarly in somata and in dendrites ($p = 0.844$, Wilcoxon signed-rank test). Data are normalized to the habituation day. **(D)** CS response amplitude test over habituation ratio in somata and dendrites. During fear conditioning, the CS response amplitude increases in somata ($p = 0.223$, Wilcoxon signed-rank test) and in dendrites ($p = < 0.001$, Wilcoxon signed-rank test, $n = 110$ soma-dendrite pairs from 17 somata). CS response probability increases similarly in somata and in dendrites ($p = 0.664$, Wilcoxon signed-rank test, $n = 110$ soma-dendrite pairs from 17 somata). Data are normalized to the habituation day. **(E)** CS response probability test over habituation ratio in somata and dendrites. During fear conditioning, the CS response probability of CS up-downregulated neurons decreases in somata ($p = 0.001$, Wilcoxon signed-rank test) but not in dendrites ($p = 0.812$, Wilcoxon signed-rank test). CS response probability ratio is higher in dendrites than in somata ($p = 0.0181$, Wilcoxon signed-rank test). Data are normalized to the habituation day. **(F)** CS response amplitude test over habituation ratio in somata and dendrites. During fear conditioning, the CS response amplitude tends to decrease in somata ($p = 0.579$) but not

in dendrites ($p = 0.466$, Wilcoxon signed-rank test, $n = 70$ soma-dendrite pairs from 16 somata). CS response probability is not significantly different in somata and in dendrites ($p = 0.262$, Wilcoxon signed-rank test, $n = 70$ soma-dendrite pairs from 16 somata). Data are normalized to the habituation day. Box-and-whisker plots show median values and $25^{th}$ and $75^{th}$ percentiles, the maximum whiskers length is 1.5 times the interquartile range.

# Discussion

As the intricate relationship between *in vivo* somatic and dendritic activity has just started to be investigated in recent years, how dendritic activity develops during learning and how it relates to changes occurring in the soma remains largely unexplored. We performed chronic imaging of somatic and dendritic $Ca^{2+}$ activity in LA PNs during fear conditioning, allowing us to probe the development of CS representation across neuronal compartments in single neurons. Like others (*54*, *55*), we observe that under baseline conditions the activity of somata and dendrites of LA PNs is strongly coupled, indicating that $Ca^{2+}$ activity spreads through the neuronal compartment efficiently. This is in contrast to the situation *in vitro,* where dendritic activity can be reliably evoked and somatic EPSPs measured in the absence of somatic firing. Our results therefore indicate that somatic and dendritic activity appears more strongly coupled *in vivo* than *in vitro.* Important differences in the experimental settings likely contribute to explain this discrepancy and should serve to emphasize that while *in vitro* studies offer unmatched access to record and manipulate neuronal activity at fine spatiotemporal scales, the putative mechanisms they uncover necessitate confirmation from experiments performed in a more physiological setting.

In this study, we observe that while somatic and dendritic activity are strongly coupled, dendrite-specific activity is increased during tone presentations. SST interneuron activity suppression abolishes this effect and increases spontaneous dendritic activity, unmasking their role in gating dendritic integration in LA PNs. Upon auditory fear conditioning, we observed bidirectional plasticity of somatic CS response, ultimately resulting in CS response stability at the population level. In stark contrast, the net CS response of dendrites and spines increased upon fear learning, suggesting compartment-specific plasticity. Consistently, we found that the CS response becomes more variable in dendrites and that somatic and dendritic activity become more decorrelated upon fear conditioning. We identified a population of neurons with decreased somatic, but stable dendritic CS response (CSdown neurons). In these neurons, somatic and dendritic plasticity of CS response follow a different course over learning, indicating compartment-specific plasticity.

Our work reveals that most $Ca^{2+}$ transients in LA PNs occur concurrently in the soma and in the dendrites of the same neurons (Fig. 18B). These findings are in line with recent studies in the neocortex reporting that the fraction of $Ca^{2+}$ transients restricted to dendrites is relatively small (*55*, *62*, *63*), and indicate a strong functional coupling between soma and dendrites. Pervasive global $Ca^{2+}$ transients could reflect efficient somatic action potential back-propagation into the dendritic arbor of PNs. However, the temporal resolution of the currently available $Ca^{2+}$ sensors do not permit to decipher the causality of somatic and dendritic activity. Faster indicators such as voltage indicators will be more suitable to characterize the directionality and the general relationship between the activity in different neuronal compartments.

Nonetheless, we observed that in the LA, the correlation between the amplitude of co-occurring somatic and dendritic $Ca^{2+}$ transients was variable within single neurons and that local dendritic activity sometimes occurred independently from somatic activity (Fig. 16D-E, Fig. 18B). The proportion of dendrite-specific $Ca^{2+}$ transients was notably higher during tones (Fig. 18B), showing that dendrites of LA PNs can be active independently from their somata and pointing to local integration of auditory inputs in dendrites.

In cortex and in cortex-like regions including the basolateral amygdala, PN dendritic activity is regulated by dendrite-targeting interneurons (*23*, *70*, *71*). SST interneurons, in particular, predominantly contact PN dendrites and provide input-specific inhibition to PNs (*24*, *72*), putting SST interneurons in an ideal position to control dendritic activity in PNs and to potentially gate dendritic integration in a stimulus-specific manner. In addition, SST interneurons activity is reduced during CS presentation in the amygdala, where it is required for fear learning and LTP (*24*). We showed that pharmacological suppression of SST interneurons decorrelates the activity of dendrites and somata in single PNs and increases the proportion of spontaneous, dendrite-specific $Ca^{2+}$ transients (Fig. 20J-K), providing evidence that activity compartmentalization in LA PN dendrites is indeed controlled by local SST inhibitory interneurons. It is possible that while the suppression of SST interneuron activity during tones results in increased dendritic excitability, SST interneurons suppress other, less salient inputs to PN dendrites. By suppressing SST activity during tone presentation, we unmasked their role in gating dendritic integration of sensory inputs.

Upon fear conditioning, the somatic CS response of LA PNs remained stable at a population level, but single neuron dynamics revealed that somatic CS responses develop bidirectionally during learning (Fig. 25A-B). However, LA PN dendrites and spines predominantly upregulated their CS response upon fear conditioning (Fig. 27B-C, Fig. 29B-C), indicating a more unidirectional plasticity of CS response in dendrites. In contrast, in pseudo-conditioned mice, CS responses of somata and dendrites decreased uniformly. These results indicate that explicit CS-US pairing induces dendritic plasticity of CS responses that are not fully reflected in somata and thus raise the question of how CS responses develop in individual dendrites and somata of single neurons.

To explore the relationship between somatic and dendritic CS responses, we considered soma-dendrite pairs of CSup and CSdown neurons and found that while the somata and dendrites of CSup neurons increased their CS responses, the dendritic responses in CSdown neurons did not decrease but instead remained stable during learning (Fig. 31D-F), leading to an uncoupling of somatic and dendritic plasticity of CS responses. Like others (*51*), we observed that CSup and CSdown neurons were similarly likely to be US-responsive (Fig. 26 F-G), arguing against Hebbian learning in the context of fear conditioning. Instead, uncoupling of CSdown CS responses in somata and in dendrites points to the role of local inhibitory interneurons directly or indirectly controlling PN somatic output (*24*, *25*).

It has been observed that during fear conditioning, GABAergic synapses in the amygdala undergo significant reorganization, resulting in a network-wide remodeling of the excitation/inhibition balance (*68*, *73*). While inputs conveying tone CSs strengthen the response of (*74*), inhibitory interneurons undergo functional reorganization during learning and dampen LA PNs somatic responses (*25*, *75*). Stimulus-specific dendritic response strengthening along with stimulus-specific somatic inhibition could be a hallmark of network reorganization during the formation of new associations while allowing the preservation of homeostasis (*76*, *77*). In this context, our results potentially bring together two apparently conflicting correlates of auditory fear learning: the long-term potentiation of auditory inputs from auditory regions of the cortex and thalamus onto the LA PNs (*78-82*) and the bidirectional functional plasticity of LA PNs CS responses (*51*). Indeed, Hebbian models predict that only neurons that respond to both CS and US during fear conditioning

should increase their CS response. Along the same line, long-term potentiation of inputs conveying the CS should then produce CSup, but not CSdown neurons (*78*, *83*). These predictions did not hold, emphasizing the limitations of classical models. Hebbian learning does not factor in the contribution of local inhibitory interneurons, nor the plasticity occurring in different neuronal compartments and therefore fails to appropriately describe indirect network effects, such as the mechanisms underlying homeostasis (*84*).

Recording activity in dendrites and somata simultaneously allows us to investigate signal transformation within a brain region and thereby delineate local and upstream circuit plasticity. Our data suggest that dendrites actively shape incoming sensory input during learning, and that somatic output does not necessarily mirror dendritic plasticity. Compartment-specific long-term changes can therefore occur in these circuits, as evidenced by the emergence of CSup and CSdown neurons, resulting in modified input-output without necessarily altering the amygdala's gross activity. According to this notion, the input-output pattern of the amygdala, rather than its overall activity level, informs downstream structures and ultimately participates to favor a particular behavior, e.g. active versus passive response to a stimulus.

It is yet unclear what factors determine the direction and the amplitude of single neuron stimulus response plasticity during learning. Some studies point to the importance of a neuron's intrinsic excitability at the time of memory formation (*85*), axonal target region (*86*, *87*) and to the role of inhibitory interneurons embedded in local microcircuits (*24*, *25*).

Importantly, neuronal networks are highly dynamic. Given the high baseline turnover rate of synaptic connections, establishing the specificity of activity changes during learning has proven to be challenging. While appropriate controls are necessary to account for the effects of habituation and the passage of time, the intrinsic variability of neuronal activity and synaptic rearrangement should also be accounted for (*88*). In addition, as motor-related signals are broadcasted throughout the brain, appropriate ways to delineate motor-related changes from specific, task-related activity is required (*89*).

Another level of specificity that requires attention concerns the physical localization of neuronal computations in the brain. Where does learning occur? From functional brain

imaging studies, we know that brain regions operate as synchronized brain-wide networks. However, with the currently available techniques, recording neuronal activity with single-cell resolution is often limited to a specific brain region and therefore comes with the price of ignoring other relevant brain areas. As a consequence, the recorded neurons report neuronal computations that likely involve other brain regions, and we have no means of isolating the contribution of the recorded region. This is particularly problematic when recording activity from neurons that are several synapses away from both sensory and motor neurons. In this regard, comparing dendritic activity to neuronal output can help establish the input-output relationship of neurons in a specific brain region.

Going further, in order to reach a mechanistic understanding of the neuronal activity changes that occur during learning, it will also be important to determine more accurately at which what timescales these changes happen, since different timescales likely reflect different biological mechanisms.

Short-term plasticity refers either to a decrease in the availability of neurotransmitters available in axon terminals (short-term depression) or to a facilitation (short-term potentiation) of neurotransmitter release due to increased $Ca^{2+}$ into the axon terminal after spike generation (*90*, *91*) and has been proposed to support working memory (*92*, *93*). In contrast, long-term potentiation is believed to underlie long-term memory (*94*, *95*). Overnight memory consolidation likely involve yet additional mechanisms, such as activity replay and brain oscillations (*52*).

Insights could be gained by putting the changes observed at the level of cellular compartments in perspective with the surrounding network activity in order to better understand the complex interactions between single neuron and network-level activity dynamics (*96*, *97*). Homeostasis, for example, has been proposed as a mechanism to counterbalance putative runaway synaptic plasticity and regulate single cell synaptic weights to normalize firing rate, with consequences on network activity regulation (*84*).

The understanding of how neuronal activity relates to the acquisition, storage and expression of new memories is still at its infancy and should be addressed at different spatial, temporal and anatomical scales. In the future, compartment-specific investigation of the role

of neuronal microcircuit elements might reveal general principles of network organization and dynamics underlying the encoding and storage of newly formed memories.

# References


1. M. S. Fanselow, A. M. Poulos, *Annu. Rev. Psychol.* **56**, 207–234 (2005).
2. H. López-Schier, *Curr. Opin. Neurobiol.* **54**, 134–139 (2019).
3. K. D. Kimura, K. Fujita, I. Katsura, **30**, 16365–16375 (2010).
4. D. Marr, *Vision: a computational investigation into the human representation and processing of visual information.* (1982).
5. B. A. Richards *et al.*, *Nat. Neurosci.* **22**, 1761–1770 (2019).
6. H. S. Seung, *Nat. Neurosci.* **3**, 1166 (2000).
7. H. Yanagisawa, O. Kawamata, K. Ueda, **13** (2019), doi:10.3389/fncom.2019.00002.
8. A. G. B. Sutton, Richard S., *Reinforcement Learning : An Introduction* (seond edit., 2018).
9. W. Schultz, P. Dayan, P. R. Montague, **275**, 1593–1600 (1997).
10. J. E. Dunsmoor, R. Paz, *Biol. Psychiatry*. **78**, 336–343 (2015).
11. J. Haaker *et al.*, *Neurosci. Biobehav. Rev.* **107**, 329–345 (2019).
12. P. Cognigni, J. Felsenberg, S. Waddell, *Curr. Opin. Neurobiol.* **49**, 51–58 (2018).
13. A. H. Taub, Y. Shohat, R. Paz, *Nat. Commun.* **9**, 1–11 (2018).
14. S. Maren, G. J. Quirk, *Nat. Rev. Neurosci.* **5**, 844–852 (2004).
15. T. Agren, (2012), doi:10.1126/science.1223006.
16. by D. G. R. A. Amaral, *Living without an Amygdala* (Guilford P., 2016).
17. K. M. McCullough, F. G. Morrison, J. Hartmann, W. A. Carlezon, K. J. Ressler, *eNeuro*. **5**, 1–12 (2018).
18. P. H. Janak, K. M. Tye, B. Sciences, C. Sciences, *Nature.Com*. **517**, 284–292 (2015).
19. J. Ledoux, **17**, 868–874 (2004).
20. E. A. Phelps, J. E. LeDoux, *Neuron*. **48**, 175–187 (2005).
21. M. Aggarwal *et al.*, *Targeted disruption of cocaine-activated nucleus accumbens neurons prevents context-specific sensitization* (2015), vol. 35.
22. J. P. Johansen *et al.*, *Proc. Natl. Acad. Sci. U. S. A.* **107**, 12692–12697 (2010).
23. S. Krabbe, J. Gründemann, A. Lüthi, *Biol. Psychiatry*. **83**, 800–809 (2018).
24. S. B. E. Wolff *et al.*, *Nature*. **509**, 453–8 (2014).
25. S. Krabbe *et al.*, *Nat. Neurosci.* **22**, 1834 (2019).
26. C. L. and R. C. Malenka2, *IEEE Technol. Soc. Mag.* **28**, 3 (2009).
27. M. Bosch *et al.*, *Neuron*. **82**, 444–459 (2014).
28. F. Hecht, B. K. McCaw, D. Peakman, A. Robinson, *Nature*. **255**, 243–244 (1975).
29. B. E. Herring, R. A. Nicoll, *Annu. Rev. Physiol.* **78**, 351–365 (2016).
30. S. C. Ramesh Rajan, in *Physiology* (Monash University, ed. 2011, 2011).
31. R. A. Nicoll, *Neuron*. **93**, 281–290 (2017).
32. T. D. Aumann, S. J. Redman, M. K. Horne, *Neurosci. Lett.* **287**, 151–155 (2000).

33. T. Sigurdsson, V. Doyère, C. K. Cain, J. E. LeDoux, *Neuropharmacology*. **52**, 215–227 (2007).

34. G. Cantarero, B. Tang, R. O'Malley, R. Salas, P. Celnik, *J. Neurosci.* **33**, 4634–4641 (2013).

35. S. M. Rodrigues, G. E. Schafe, J. E. Ledoux, *Neuron*. **44**, 75–91 (2004).

36. G. L. Dalton, D. Chuan, Y. Tian, S. B. Floresco, A. G. Phillips, *Neuropharmacology*. **62**, 797–806 (2012).

37. S. Nabavi *et al.*, *Nature*. **511**, 348–352 (2014).

38. Y. Bengio, T. Mesnard, (2015).

39. K. He *et al.*, *Neuron*. **88**, 528–538 (2015).

40. G. Bi, M. Poo, *Annu. Rev. Neurosci.* **24**, 139–166 (2001).

41. I. A. Lazarevich, V. B. Kazantsev, 2–6.

42. H. C. Lai, L. Y. Jan, *Nat. Rev. Neurosci.* **7**, 548–562 (2006).

43. A. Losonczy, J. C. Magee, *Neuron*. **50**, 291–307 (2006).

44. H. Markram *et al.*, 409–440 (1997).

45. M. London, M. Häusser, *Annu. Rev. Neurosci*. **28**, 503–535 (2005).

46. S. Tazerart, D. E. Mitchell, S. Miranda-Rottmann, R. Araya, *bioRxiv*, 397323 (2018).

47. G. J. Stuart, N. Spruston, *Nat. Neurosci.* **18**, 1713–1721 (2015).

48. M. Raffi, C. Carrozzini, M. G. Maioli, S. Squatrito, *Neuroscience*. **171**, 1241–1255 (2010).

49. P. Kyriazi, D. B. Headley, D. Pare, *Neuron*. **99**, 1–14 (2018).

50. E. Seidemann, W. S. Geisler, 287–310 (2018).

51. B. F. Grewe *et al.*, *Nature*. **543**, 670–675 (2017).

52. J. G. Klinzing, N. Niethard, J. Born, *Nat. Neurosci.* **22** (2019), doi:10.1038/s41593-019-0467-3.

53. J. Cichon, W. B. Gan, *Nature*. **520**, 180–185 (2015).

54. V. Francioni, N. L. Rochefort, N. Rochefort, "High somato-dendritic coupling of V1 layer 5 neurons independent of behavioural state and visual stimulation."

55. L. Beaulieu-Laroche, E. H. S. Toloza, N. J. Brown, M. T. Harnett Correspondence, *Neuron*. **103**, 1–7 (2019).

56. H. Taniguchi *et al.*, *Neuron*. **71**, 995–1013 (2011).

57. C. Xu *et al.*, *Cell*. **167**, 961-972.e16 (2016).

58. M. H. Longair, D. A. Baker, J. D. Armstrong, *Bioinforma. Appl. NOTE*. **27**, 2453–2454 (2011).

59. A. Rahmanian-Schwarz *et al.*, *J. Investig. Surg.* **25**, 123–126 (2012).

60. E. A. Pnevmatikakis, A. Giovannucci, *J. Neurosci. Methods*. **291**, 1–12 (2017).

61. Keith Frankin, G. Paxinos, *The Mouse Brain in Stereotaxic Coordinates, Volume 1* (Academic Press, second., 2001).

62. V. Francioni, Z. Padamsey, N. L. Rochefort, *Elife*. **8**, 1–25 (2019).

63. A. Kerlin *et al.*, *Elife*. **8**, 1–33 (2019).

64. C. Q. Chiu *et al.*, *Science*. **340**, 759–62 (2013).

65. B. L. Roth, *Neuron*. **89**, 683–694 (2016).

66. X. Zhang, B. Li, *Neuron*. **100**, 780–782 (2018).

67. Y. Kasugai *et al.*, *Neuron*. **104**, 781-794.e4 (2019).

68. P. Botta *et al.*, *Nat. Neurosci.* **18**, 1493–1500 (2015).

69. G. P. McNally, J. P. Johansen, H. T. Blair, *Trends Neurosci.* **34**, 283–292 (2011).

70. J. J. Letzkus *et al.*, *Nature*. **480**, 331–335 (2011).

71. E. Abs *et al.*, (2018), doi:10.1016/j.neuron.2018.09.001.

72. C. Q. Chiu *et al.*, *Science (80-. ).* **340**, 759–762 (2013).

73. E. V. Yu Kasugai, N. S. Heide Ho¨rtnagl, ..., F. F. Andreas Luthi.

74. S. Maren, *Trends Neurosci.* **22**, 561–567 (1999).

75. A. Puścian, H. Benisty, M. J. Higley, *bioRxiv* (2019), doi:10.1101/688366.

76. A. G. Khan *et al.*, *Nat. Neurosci.* **21**, 851–859 (2018).

77. D. E. Wilson, B. Scholl, D. Fitzpatrick, *Nature*. **560**, 97–101 (2018).

78. H. T. Blair, G. E. Schafe, E. P. Bauer, S. M. Rodrigues, J. E. LeDoux, *Learn. Mem.* **8**, 229–242 (2001).

79. C. W. Butler *et al.*, **10**, 114–18 (2018).

80. S. Maren, *Annu. Rev. Neurosci.* **24**, 897–931 (2001).

81. M. T. Rogan, U. V Stäubli, J. E. LeDoux, *Nature*. **390**, 604–7 (1997).

82. M. Poo *et al.*, *BMC Biol.* **14**, 40 (2016).

83. E. P. Bauer, J. E. LeDoux, K. Nader, *Nat. Neurosci.* **4**, 687–688 (2001).

84. J. Yin, Q. Yuan, **8**, 1–8 (2015).

85. A. P. Yiu *et al.*, *Neuron*. **83**, 722–735 (2014).

86. P. Namburi *et al.*, *Nature*. **520**, 675–678 (2015).

87. A. Beyeler *et al.*, *Cell Rep.*, 905–918 (2018).

88. D. Shimaoka, N. A. Steinmetz, K. D. Harris, M. Carandini, *Elife*. **8**, 1–19 (2019).

89. D. B. Salkoff, E. Zagha, E. McCarthy, D. A. McCormick, *Cereb. Cortex*. **30**, 421–437 (2020).

90. H. Markram, M. Tsodyks, **382**, 807–810 (1996).

91. L. F. Abbott, J. A. Varela, K. Sen, S. B. Nelson, *Science (80-. ).* **275**, 220–224 (1997).

92. D. Hansel, G. Mato, *J. Neurosci.* **33**, 133–149 (2013).

93. A. Seeholzer, M. Deger, W. Gerstner, *Stability of working memory in continuous attractor networks under the control of short-term plasticity* (2018).

94. D. Norris, *Psychol. Bull.* **143**, 992–1009 (2017).

95. R. Stickgold, M. P. Walker, *Trends Neurosci.* **28**, 408–415 (2005).

96. D. Feldmeyer, G. Qi, V. Emmenegger, J. F. Staiger, *Neuroscience*. **368**, 132–151 (2018).

97. M. E. Hasselmo, **16**, 710–715 (2009).

# Acknowledgements

I would like to thank Andreas Lüthi for giving me the opportunity to enter the captivating world of neuroscience and for his constant support and trust, especially during challenging times. Thanks also to Tiago Branco for his advice. Thank you to the Lüthi lab as a whole, eclectic gathering of exceptional individuals, for being what it is, an always changing but always welcoming community that I shared and still share a lot with. In particular, I want to thank Jan Gründemann and Sabine Krabbe for their help, guidance and benevolence all along my PhD. Thank you also to Iris Odstrcil for proof-reading the present thesis. The FMI is a great, stimulating environment to do science, with dense interactions and amazing facilities that make everyone's life easier. I want to thank Jan Eglinger, Steven Bourke and Raphael Thierry from the imaging facility for their active contribution to my projects, always attuned the specific needs and optimistic in their attitudes. Likewise, I want to all animal caretakers and in particular Gisele Ferrand for looking after our precious mice, always adapting to our changing needs with flexibility and a positive attitude. I want to thank my friends and family from Strasbourg and beyond, always present and supportive, reminding me what life looks like outside of the mouse house. Finally, I thank my fiancée Shuting Han, putting up with me all along with great tolerance, love and support. She changed everything.

# Curriculum vitae


## Simon d'Aquin

Weinberstrasse 68
8006 Zürich, Switzerland
simondaquin@gmail.com
+41(0)793267822


### Personal

| | |
|---|---|
| Birth date: | 29th June 1990. |
| Citizenship: | French Citizen. B permit (Switzerland) |
| Marital Status: | Single |
| Languages: | English: C1, German: B1, French: native |

### *Education*

9/2014 – present **Friedrich Miescher Institute, University of Basel**

Graduate student with Prof. Andreas Lüthi

PhD thesis title: "Compartment-specific plasticity in the lateral amygdala during fear learning"

- Two-photon microscopy
- Neuronal activity analysis
- Whole-brain anatomical tracing
- Whole-cell patch-clamp recording
- Animal behaviour

*9/2010 – 9/2013* **Ecole Supérieure de Biotechnologie de Strasbourg (ESBS)**

Engineer Diploma in Biotechnology, equivalent to MSc

- Trinational school (English/German/French)
- Genetic engineering, microbiology

*9/2008 – 9/2010* **Faculty of Life Sciences, University of Strasbourg**

- Biochemistry
- molecular biology

### *Experience*

*1/2014 – 6/2014* **Novartis Institutes for Biomedical Research (NIBR), Basel**

Research Associate

Characterization of new genes and chemical compounds involved in mitochondrial autophagy (Dowdle et al., 2014).

*1/2013 – 12/2013* **Master thesis**

Developed a high-throughput image-based assay for RNAi screening.
Identified new genes involved in the regulation of mitochondrial autophagy.

*7/2012 – 8/2012* **Max-Planck-Institut für experimentelle Medizin, Göttingen**

Rotation Student with Dr. Sandra Goebbels
Identified a strong myelination phenotype in PTEN/BDNF double knocked out mice cerebellum.

*12/2012* **Centre of Biological Signalling Studies (BIOSS), Freiburg**
Master Student with Prof. Wilfried Weber
Design and production of new chimeric sensor/reporter proteins.

*7/2011 – 8/2011* **Alaxia Pharma, Lyon**
Lab Assistant with Dr. Sandrine Perrotto
Synthesis and evaluation of a candidate drug activity on multi-resistant bacterial strains.

*7/2010* **UMR7242 Biotechnology and cell signalling, University of Strasbourg**
Lab Assistant with Dr. Valérie Geoffroy
Production of bacterial siderophores library from multiple bacterial strains.

## *Publications*

Adaptive disinhibitory gating by VIP interneurons permits associative learning. *Krabbe S, Paradiso E, d'Aquin S, Bitterman Y, Courtin J, Xu C, Yonehara K, Markovic M, Müller C, Eichlisberger T, Gründemann J, Ferraguti F, Lüthi A.* Nat Neurosci. 2019 Nov;22(11):1834-1843. doi: 10.1038/s41593-019-0508-y. Epub 2019 Oct 21. PMID: 31636447

Selective VPS34 inhibitor blocks autophagy and uncovers a role for NCOA4 in ferritin degradation and iron homeostasis in vivo. *Dowdle WE, Nyfeler B, Nagel J, Elling RA, Liu S, Triantafellow E, Menon S, Wang Z, Honda A, Pardee G, Cantwell J, Luu C, Cornella-Taracido I, Harrington E, Fekkes P, Lei H, Fang Q, Digan ME, Burdick D, Powers AF, Helliwell SB, D'Aquin S…, Murphy LO.* Nat Cell Biol. 2014 Nov;16(11):1069-79. doi: 10.1038/ncb3053. Epub 2014 Oct 19. PMID: 25327288

## Talks

03/2020 Institute of Pharmacology and Toxicology, University of Zürich, Switzerland
"Compartment-specific plasticity in the lateral amygdala during fear learning"

02/2020 Swiss Society for Neuroscience 2020 meeting, Bern, Switzerland
"Dendritic integration in the Lateral Amygdala during auditory fear conditioning"

01/2020: Neuroseminar, Friedrich Institute for Neuroscience, Basel, Switzerland
"Compartment-specific plasticity in the lateral amygdala during fear learning"

## Posters

11/2019 Fear learning symposium, EPFL, Switzerland
"Compartment-specific plasticity in the lateral amygdala during fear learning"
d'Aquin S. 1, Krabbe, S. Gründemann J. & A.Lüthi

03/2019 Dendrites Gordon Conference, Ventura, CA, USA
"Dendritic integration in the lateral amygdala during auditory fear conditioning"

d'Aquin S. 1, Krabbe, S. Gründemann J. & A.Lüthi

09/2016 Probing neuronal circuits during behavior, Bordeaux, France
"Mechanisms of dendritic integration in the lateral amygdala during learning"
d'Aquin S. 1, Krabbe, S. Gründemann J. & A.Lüthi

*"I hereby declare that this doctoral dissertation 'Compartment-specific plasticity in the lateral amygdala during fear learning' has been completed exclusively with the assistance mentioned herein and that it has not been submitted to any other university or to any other faculty at the University of Basel."*

*Simon d'Aquin, 15 December 2020*